Leukemia inhibitory factor is a therapeutic target for renal interstitial fibrosis

*Shihui Xu,[a] Xiaobing Yang,[a] Qingzhou Chen, Zhuoliang Liu, Ying Chen, Xiaotian Yao, An Xiao, Jianwei Tian, Liling Xie, Miaomiao Zhou, Zheng Hu, Fengxin Zhu, Xin Xu, Fanfan Hou,** and Jing Nie**

Division of Nephrology, State Key Laboratory of Organ Failure Research, National Clinical Research Center of Kidney Disease, Guangdong Provincial Institute of Nephrology, Guangdong Provincial Key Laboratory of Renal Failure Research, Nanfang Hospital, Southern Medical University, Guangzhou, China

eBioMedicine
2022;86: 104312
Published Online XXX
https://doi.org/10.1016/j.ebiom.2022.104312

Summary

Background The role of the IL6 family members in organ fibrosis, including renal interstitial fibrosis (TIF), has been widely explored. However, few studies have ever simultaneously examined them in the same cohort of patients. Besides, the role of leukemia inhibitory factor (LIF) in TIF remains unclear.

Methods RNA-seq data of kidney biopsies from chronic kidney disease (CKD) patients, in both public databases and our assays, were used to analyze transcript levels of IL6 family members. Two TIF mouse models, the unilateral ureteral obstruction (UUO) and the ischemia reperfusion injury (IRI), were employed to validate the finding. To assess the role of LIF in vivo, short hairpin RNA, lenti-GFP-LIF was used to knockdown LIF receptor (LIFR), overexpress LIF, respectively. LIF-neutralizing antibody was used in therapeutic studies. Whether urinary LIF could be used as a promising predictor for CKD progression was investigated in a prospective observation patient cohort.

Findings Among IL6 family members, LIF is the most upregulated one in both human and mouse renal fibrotic lesions. The mRNA level of LIF negatively correlated with eGFR with the strongest correlation and the smallest *P* value. Baseline urinary concentrations of LIF in CKD patients predict the risk of CKD progression to end-stage kidney disease by Kaplan–Meier analysis. In mouse TIF models, knockdown of LIFR alleviated TIF; conversely, overexpressing LIF exacerbated TIF. Most encouragingly, visible efficacy against TIF was observed by administering LIF-neutralizing antibodies to mice. Mechanistically, LIF–LIFR-EGR1 axis and Sonic Hedgehog signaling formed a vicious cycle between fibroblasts and proximal tubular cells to augment LIF expression and promote the pro-fibrotic response via ERK and STAT3 activation.

Interpretation This study discovered that LIF is a noninvasive biomarker for the progression of CKD and a potential therapeutic target of TIF.

Fundings Stated in the Acknowledgements section of the manuscript.

Keywords: IL6 family; LIF; Renal fibrosis; Chronic kidney disease; Fibroblast activation

Introduction

Chronic kidney disease (CKD) is a worldwide public health problem associated with high morbidity and mortality as well as high health care costs.[1,2] Clinically, there are few available strategies to manage CKD other than dialysis or kidney transplantation. Renal tubule interstitial fibrosis (TIF) is the terminal manifestation and common pathway by which CKD progresses to end stage, which is characterized by expansion of the space between tubular basement membrane and peritubular capillaries through deposition of extracellular matrix (ECM).[3,4] Activated fibroblasts have been recognized as the major contributor of ECM during the process of TIF.[5] In addition, activated fibroblasts produce soluble

*Corresponding author. Division of Nephrology, Nanfang Hospital, Southern Medical University, Guangzhou, China.
**Corresponding author. Division of Nephrology, Nanfang Hospital, Southern Medical University, Guangzhou, China.
E-mail addresses: ffhouguangzhou@163.com (F. Hou), niejing@smu.edu.cn (J. Nie).
[a]These authors contribute to this work equally.

Research in context

Evidence before this study

Renal tubule interstitial fibrosis (TIF) is the terminal manifestation and common pathway by which CKD progresses to end stage. The role of IL6 family members in the pathogenesis of organ fibrosis including TIF has been studied extensively. Different members of the IL6 family are highly expressed in different cells in diverse organs and play various roles in fibrosis. Therefore, the role of each member in each organ needs to be explored. However, few study has ever evaluated the expression of all IL6 family member simultaneously in the same model of TIF. LIF is a member of the IL6 family. Heart-specific overexpression of LIF caused cardiac hypertrophy. Transgenic mice expressing LIF from the insulin promoter displayed considerable interstitial fibrosis throughout the pancreas. In TIF, one research found adding extrinsic LIF protein could alleviate fibrosis while another founded it makes no difference. Hence the role of LIF in TIF remains unclear.

Added value of this study

We initiated to compare the expression level of IL6 family members in the same animal models of TIF and the same cohort of CKD patients. Using RT-PCR, we identified LIF as the most upregulated IL6 family member in the fibrotic renal lesions induced by UUO and IRI in mice. This finding was confirmed by analyzing published RNA-seq (GSE98622, GSE118339) and MS data (GSE126182). To evaluate the expression of IL6 family members in human TIF, we conducted RNA-seq analysis of renal biopsies from a cohort of CKD patients. We found that LIF is the most upregulated one in human renal fibrotic lesions. Importantly, the mRNA level of LIF negatively correlated with eGFR with the strongest correlation and the smallest *P* value among IL6 family members. In patients with biopsy-confirmed IgA nephropathy, only LIF mRNA expression significantly correlated with the severity of TIF shown as the Oxford MEST-T grade. The expression of IL6 family members and their associations with TIF/eGFR were confirmed by the ERCB Nephrotic Syndrome Data set of Nephroseq V5 transcriptomic database. The baseline LIF concentration in the urine of CKD patients significantly correlated with the increased risk of progression to end-stage kidney disease. Via analyzing published single nucleus RNA sequencing (snRNA-seq) dataset of fibrotic kidney from mice 14 days after UUO (GSE119531) and a published Smart-Seq dataset of PDGFRβ$^+$ cells from mice 10 days after UUO (https://zenodo.org/record/4059315, https://doi.org/10.5281/zenodo.4059315), we found that LIF was mainly expressed in activated fibroblast, proliferating proximal tubule epithelial cells and collecting duct-principal cells. While, LIFR was ubiquitously expressed in variety of cells. Mechanistically, LIF–LIFR-EGR1 axis and Sonic Hedgehog signaling formed a vicious cycle between fibroblasts and proximal tubular cells to augment LIF expression and promote the pro-fibrotic response via ERK and STAT3 activation. LIF promoted macrophage infiltration and the phenotype transition toward pro-fibrotic phenotype. In mice models of TIF, knockdown of LIFR with short hairpin RNA alleviated TIF, while ectopic expression of LIF triggered TIF. In therapeutic studies, a LIF-neutralizing antibody attenuated TIF.

Implications of all the available evidence

This study indicated that LIF is a noninvasive biomarker for assessing the state of kidney fibrogenesis and a potential therapeutic target of TIF.

ligands which have paracrine effects on tubular epithelial cells (TECs) to interfere with the adaptive repair of damaged TECs.[6,7] On the other hand, maladaptive repaired TECs release various soluble ligands to promote fibroblasts proliferation and activation.[8–10] Hence, disrupting the vicious cycle between TECs and fibroblasts is a potential approach to impede the progression of TIF.

Among cytokine families, the IL6 cytokines family, which comprises IL6, IL11, IL27, IL31, oncostatin M (OSM), LIF, ciliary neurotrophic factor (CNTF), cardiotrophin 1 (CTF1) and cardiotrophin-like cytokine factor 1 (CLCF1), displays the highest degree of functional pleiotropy in many physiological and pathological processes, and often act as diagnostic or prognostic indicators of disease activity.[11,12] However, the role of IL6 family members in the pathogenesis of CKD needs further investigation. For example, IL6 elicits defined impact on inflammation, and has been implicated in the pathogenesis of various chronic inflammatory diseases including rheumatoid arthritis (RA),[13] Castleman's disease[14] and osteoporosis.[15] Given the mechanistic rationale for the role of IL6 in inflammation,[16–18] it has been proposed that IL6 might contribute to organ fibrosis. However, the effect of genetic depletion of IL6 on different experimental models of renal fibrosis were inconsistent.[19,20] On the other hand, most recent studies highlight the pro-fibrotic function of IL11 in the process of cardio-renal and pulmonary fibrosis.[21,22] IL27, which is mainly produced by antigen-presenting cells, has been shown to have pro and anti-inflammatory effect.[23,24] IL27 receptor α (IL27Rα) deficiency resulted in increased renal injury and collagen deposition associated with increased interstitial inflammation after UUO.[25] LIF has been reported to have paradoxically opposite effects depending on cell type and developmental stage.[26] In the case of CKD, the upregulation of renal LIF has been observed, while its role in the pathogenesis of TIF remains unclear.[27] Collectively, these findings indicate that the precise function of individual

IL6 family member in the pathogenesis of TIF needs to be dissected carefully. In addition, although the upregulation of various IL6 family member has been reported in various animal models of CKD or human CKD,[21,25,27–30] all the studies have been conducted separately for each member. Whether any of IL6 family member could serve as a biomarker of CKD remains unclear.

In the current study, we systemically evaluated the expression of all IL6 family members in renal biopsy specimens of a cohort of patients with CKD and preclinical mouse models of TIF. Surprisingly, we found that, among IL6 family members, LIF was the most upregulated one in fibrotic renal lesions. LIF has the strongest association with the extent of TIF and the decline of renal function. We dissected the pro-fibrotic role of LIF in vitro and in vivo. Furthermore, we explored the therapeutic potential of LIF-neutralizing antibody in treating TIF. Finally, using bio-samples from a prospective cohort of patients with CKD, we demonstrated the potential role of urinary LIF as a promising biomarker for CKD progression.

Methods

Ethics statement

The study was approved by the Institutional Review Board of the National Clinical Research Center for Kidney Disease (Guangzhou, China) (NO. NFEC-2019-209 and NFEC-2019-094). All of the study participants provided written informed consent. All animal experiments complied with the guiding principles approved by the Animal Care Ethics Committee of Nanfang Hospital (NO. NFYY-2019-0627).

Human subjects

Collection of renal biopsies for RNA-sequencing from cohort of CKD patients

A total of 33 patients with biopsy-proven IgAN and 6 patients with biopsy-proven MCD in Division of Nephrology, Nanfang Hospital were recruited for conducting RNA-seq analysis. Clinical characteristics of the 39 patients are shown in Table 1.

Measurement of urinary LIF in CKD patients

Twenty-four-hour urine was collected from biopsy-proven IgAN patients in Division of Nephrology, Nanfang Hospital. The concentrations of LIF in the urine were measured by human-specific LIF ELISA kits (DLF00B, R&D, Minneapolis, MN, USA). Clinical characteristics of IgAN patients were shown in Table 3 and healthy controls in Table 2.

A prospective observational cohort of patients with CKD was built from April 2014 to August 2020 in Division of Nephrology, Nanfang hospital. Eligible participants were clinically diagnosed CKD patients with 18 years or older and not receiving chronic dialysis or post renal transplantation. Spot urine samples and clinical data were collected at baseline per standard operational protocols in all enrolled patients. Clinical characteristics of CKD patients were shown in Table 4. The participants were followed every 3 months until August 2021. The renal outcome was defined as renal failure (need for chronic kidney replacement therapy or receiving renal transplantation). In this prospective cohort, baseline uLIF levels were measured using commercial ELISA kit (DLF00B, R&D, Minneapolis, MN, USA) and normalized for urinary creatinine and expressed as nanograms per gram of creatinine.

Gene/protein differential analysis of published data

We retrieved the published transcriptome/proteome data from the NCBI Gene Expression Omnibus (the GEO series numbers were GSE98622, GSE118339 and

Characteristics	Overall
Patients, No.	39
Gender = Male, n (%)	21 (53.8)
Age, mean (SD), yr	34.03 (12.13)
Serum creatinine, mean (SD), μmol/L	91.54 (39.09)
eGFR, mean (SD), ml/min/1.73m^2	92.24 (34.57)
eGFR levels, n (%)	
≥90	22 (56.41)
60–90	7 (17.95)
30–60	10 (25.64)
Disease, n (%)	
IgA Nephropathy	33 (84.6)
Minimal Change Disease	6 (15.4)
Interstitial fibrosis = Yes, n (%)	33 (84.6)
IgAN oxford classification-T, n (%)	
T0	12 (30.8)
T1	10 (25.6)
T2	11 (28.2)

[a]Continuous variables were presented as mean (SD), categorical variables were presented as number (percent). [b]We estimated the glomerular filtration rate (eGFR) using the CKD-EPI formula. [c]The pathological types of 33 cases of interstitial fibrosis were IgAN while 6 cases of no interstitial fibrosis were Minimal Change Disease (MCD).

Table 1: **Clinical characters of CKD patients for RNA-seq.**

Characteristics	Overall
Healthy controls, No.	8
Gender = Male, n (%)	2 (25)
Age, mean (SD), yr	27.25 (1.83)
Serum creatinine, mean (SD), μmol/L	58.625 (7.52)
eGFR, mean (SD), ml/min/1.73m^2	124.5788 (5.45)

[a]Continuous variables were presented as mean (SD), categorical variables were presented as number (percent). [b]We estimated the glomerular filtration rate (eGFR) using the CKD-EPI formula.

Table 2: **Clinical characters of healthy controls.**

Characteristics	Overall
Patients, No.	50
Gender = Male, n (%)	22 (44)
Age, mean (SD), yr	37.7 (11.04)
Serum creatinine, mean (SD), μmol/L	146.66 (137.54)
eGFR, mean (SD), ml/min/1.73m^2	68.87 (35.83)
eGFR levels, n (%)	
≥90	15 (30)
60–90	12 (24)
30–60	16 (32)
15–29	5 (10)
<15	2 (4)
IgAN oxford classification-T, n (%)	
T0	16 (32)
T1	20 (40)
T2	14 (28)

[a]Continuous variables were presented as mean (SD), categorical variables were presented as number (percent). [b]We estimated the glomerular filtration rate (eGFR) using the CKD-EPI formula.

Table 3: **Clinical characters of CKD patients for 24 h-uLIF.**

GSE126182).[31,32] We downloaded the gene/protein expression matrix from supplementary file in each GEO series website. Genes/proteins expressed in all samples of each GEO data set were included for analysis. We used the R package limma (3.46.0) for gene/protein differential expression analysis between different groups.

RNA-seq data analysis

Library preparation

For primary mouse renal tubular cells, library preparation was performed by Gene Denovo Biotechnology Co (Guangzhou, China). More specifically, total RNA was extracted using Trizol reagent kit (Vazyme Biotech Co, Ltd, China) according to the manufacturer's protocol and enriched by Oligo (dT) beads, while prokaryotic mRNA was enriched by removing rRNA by Ribo-ZeroTM Magnetic Kit (Epicentre, Madison, WI, USA). Then the enriched mRNA was fragmented into short fragments using fragmentation buffer and reverse transcripted into cDNA with random primers. Second-strand cDNA were synthesized by DNA polymerase I, RNase H, dNTP and buffer. Then the cDNA fragments were purified with QiaQuick PCR extraction kit (Qiagen, Venlo, The Netherlands), end repaired, dA-Tailing added and ligated to Illumina sequencing adapters. The ligation products were size selected by agarose gel electrophoresis, PCR amplified.

For patient samples, library preparation was accomplished by VeritasGenetics Inc (Hangzhou, China). Specifically, the transcriptome library for sequencing was generated using the VAHTS Total RNA-Seq (H/M/R) Library Prep Kit for Illumina (Vazyme Biotech Co, Ltd, Nanjing, China). The details of the library construction were similar to primary mouse renal tubular cells, including removing ribosomal RNA, RNA fragmentation, reverse transcription, dA-Tailing added and ligated to the adapter. Furthermore, the library fragments of patient samples were purified with AMPure XP system to select the appropriate cDNA fragment size for sequencing. Uridine digestion was performed using Uracil-N-Glycosylase, which was followed by the cDNA amplification using PCR. All cDNA libraries sequenced on Illumina HiSeq platform (Hiseq X10 platform for patient samples, HiSeq 2500 for primary mouse renal tubular cells).

Variable[a]	Overall	Urinary LIF (ng/g Cr)			P[b]
		T1 (<19.4)	T2 (19.4–53.5)	T3 (>53.5)	
No. of patients	362	120	121	121	–
Age, y	48.1 ± 14.1	46.2 ± 13.6	48.2 ± 14.3	50.1 ± 14.2	0.10
Men	233 (64.4%)	87 (72.5%)	85 (70.2%)	61 (50.4%)	<0.001
BMI, kg/m^2	23.9 ± 3.8	23.7 ± 3.7	24.3 ± 3.6	23.6 ± 4.2	0.21
Diabetes	61 (16.9%)	17 (14.2%)	17 (14.0%)	27 (22.3%)	0.25
Hypertension	228 (63.0%)	67 (55.8%)	74 (61.2%)	87 (71.9%)	0.13
MAP, mmHg	101.9 ± 15.5	99.1 ± 13.9	103.1 ± 15.7	103.4 ± 16.5	0.12
eGFR, ml/min/1.73m^2	36.2 ± 21.1	41.1 ± 21.4	38.2 ± 20.3	29.6 ± 19.8	<0.001
Proteinuria, g/d	2.2 ± 3.2	1.6 ± 2.2	1.4 ± 2.4	3.7 ± 4.3	<0.001
Hemoglobin, g/L	121.1 ± 21.7	126.6 ± 22.5	121.0 ± 20.7	115.6 ± 20.5	<0.001
Serum albumin, g/L	38.7 ± 7.2	40.3 ± 6.0	39.9 ± 5.8	36.1 ± 8.7	<0.001
Serum TG, mmol/L	1.8 ± 1.1	1.8 ± 1.0	1.6 ± 1.0	1.9 ± 1.1	0.09
Serum CHOL, mmol/L	4.9 ± 1.7	4.7 ± 1.6	4.6 ± 1.2	5.5 ± 2.2	0.04

Abbreviations: BMI, body mass index; CHOL, cholesterol; eGFR, estimated glomerular filtration rate; LIF, leukemia inhibitory factor; MAP, mean arterial blood pressure; T, tertile; TG, triglycerides. [a]Continuous variables are expressed as mean ± standard deviation. Categorical variables are expressed as number (percent). [b]Comparing the covariates across the 3 urinary LIF categories.

Table 4: **Characteristics of CKD patient cohort by urinary LIF levels at baseline.**

Data processing and bioinformatics analysis

RNA-Seq FASTQ raw data were processed and the clean reads were obtained by removing adapter sequences and low-quality reads from raw data using Trimmomati (version 0.39),[33] fastp (version 0.18.0).[34] Next, the clean reads were aligned to the reference genome (hg38 for human and mm10 for mouse) using STAR aligner (version 2.7.7a).[35] Uniquely mapped reads were counted using the featureCounts (version 2.0.1)[35] to quantify gene expression. RNAs differential expression analysis was performed by limma (version 3.46.0)[36] software between two different groups. The genes with the parameter of *P* value below 0.05 were considered significant differentially expressed genes.

For gene set variation analysis (GSVA), pathway analyses were predominantly performed on the 50 hallmark pathways described in the molecular signature database, exported using the msigdbr (version 7.2.1).[37] To reduce gene overlaps in each gene set, each gene set associated with a pathway was trimmed to only contain unique genes. Next, to assign pathway activity estimates to individual samples, we applied GSVA using standard settings, as implemented in the GSVA package (version 1.38.0).[38] To assess differential activities of pathways between differential samples, we contrasted the activity scores for each sample using a generalized linear model.[38] Results of these linear models were visualized using bar plots.

Analysis of published single cell RNA-seq data

The data of UUO snRNA-seq (10X)[39] and UUO PDGFRβ^{+} scRNA-seq (SmartSeq2)[40] were obtained respectively from GSE119531 and the Zenodo data archive (https://zenodo.org/record/4059315, https://doi.org/10.5281/zenodo.4059315), which contain the gene expression matrix data and cell cluster annotations. Then, we performed data normalization and scaling according to standard pre-processing workflow of the Seurat[41,42] (version 4.0, https://satijalab.org/seurat/). Dotplot was used to visualize relevant genes expression, including *Lif*, *Il11*, *Lifr*, *Il6st*, *Pdgfra*, *Pdgfrb* and *Tgfb1*.

Animal experiments

Male BALB/C and C57BL/6 mice (body weight 20–25 g and age 8–10 weeks) used in this study were purchased from Yancheng biology (Guangzhou, China). All mice were anesthetized with intraperitoneal injection of sodium pentobarbital (11715, Sigma–Aldrich, St. Louis, MO, USA) before the surgical operation.

Unilateral ureteral obstruction (UUO) was performed on the left ureter of BALB/C mice, as previously described.[43] Briefly, left ureter of the mouse was ligated twice with 4-0 silk surgical sutures at the lower pole of the kidney. Sham-operated mice had their ureters exposed, but not ligated. Mice were sacrificed on day 3, 7, or 14 after surgery. Kidney tissues were stored at –80 °C for further experimental analysis.

Ischemia reperfusion injury (IRI) in C57BL/6 mice was performed as previously described.[44] Briefly, the left kidney's pedicle was clamped for 30 min at 37 °C to completely block renal blood flow, followed by the clamp's release to restore renal blood supply to induce ischemia reperfusion injury. Mice were sacrificed on day 3, 7, or 14 after reperfusion. Unilateral ischemia reperfusion injury (UIRI) in C57BL/6 mice was performed as mentioned above and contralateral kidney was removed 1 day before the mouse was sacrificed. Kidney tissues were stored at –80 °C for further experimental analysis.

Lentiviral constructs

The constructs of lenti-LIF-GFP and lenti-shLIFR-GFP were designed and constructed by Shanghai GenePharma Co (Shanghai, China). Based on the manufacturer's instruction, four plasmid system was used for lentivirus packaging included pGag/Pol, pRev and pVSV-G, the LIFR interfering RNA sequence was 5′-GGACATCAATTCAACAGTTGT-3′. The full-length mouse LIF cDNA (NCBI Reference Sequence: NM_008501.2) was amplified and cloned into LV5 (Shanghai GenePharma Co).

Overexpression of LIF in mice

Male BALB/C mice were randomly divided into 3 groups (n = 6 in each group): (i) sham-operated group; (ii) UUO mice receiving lenti-GFP-NC; (iii) UUO mice receiving lenti-GFP-LIF. 4×10^7 transducing units of control lentivirus (lenti-GFP-NC) or lenti-GFP-LIF in 100 μl PBS were injected into left renal parenchyma through abdominal incision exposing the abdominal cavity 3 days before UUO surgery. Three days later, the left kidney was exposed through the back incision and UUO surgery was conducted. All mice were sacrificed on day 7 after surgery.

Knocking down endogenous LIFR in vivo

Male BALB/C mice were randomly divided into 3 groups (n = 6 in each group): (i) sham-operated group; (ii) UUO mice receiving lenti-Ctrl-shNC (lentiviral vector containing scrambled shRNA); (iii) UUO mice receiving lenti-LIFR-shR (lentiviral vector containing LIFR shRNA). 4×10^7 transducing units of lenti-Ctrl-shNC or lenti-LIFR-shR in 100 μl PBS were injected into renal parenchyma 4 days before UUO surgery as described above. All mice were sacrificed on day 10 after surgery.

In vivo LIF-neutralizing antibody administration

Male BALB/C or C57BL/6 mice were randomly divided into 3 groups (n = 6 in each group): (i) sham-operated group; (ii) UUO/UIRI mice receiving IgG; (iii) UUO/UIRI mice receiving LIF-neutralizing antibody. IgG

Days after UUO	3	5	7	8	9	10	11	12	13
Dosage of IgG or LIF-neutralizing antibody (mg/kg via the tail vein)	0.25	0.5	0.75	1	1.25	1.5	1.75	2	2

Table 5: **The dosage and time period of UUO mice receiving IgG or LIF-neutralizing antibody.**

(R&D Systems Cat# BAF108, RRID: AB_355828) or LIF-neutralizing antibody (R&D Systems Cat# AB-449-NA, RRID: AB_354362) was injected into mice via tail-vein injection. The dosage and time period of mice receiving IgG or LIF-neutralizing antibody was described in Tables 5 and 6. BALB/C mice were sacrificed on day 14 after UUO. C57BL/6 mice were sacrificed on day 12 after UIRI.

Renal function and histology

Renal function was assessed by measuring serum creatinine (OSR61204, Beckman Coulter, CA, USA) using an automatic biochemical analyzer (Beckman Coulter, CA, USA). 2 μm paraffin-embedded kidney sections were subjected to hematoxylin and eosin (HE), Masson trichrome and Sirius red staining using commercial kits (BA4356, BA4079B, BASO, China) according to the manufacturer's protocol. HE staining was used to assess tubular atrophy. Non-vascular parts of cortex regions were selected for fibrosis assessment. To evaluate the degree of interstitial fibrosis, Sirius red and Masson trichrome stainings were evaluated by calculating the proportion fraction of the red and blue area, respectively. The proportion fraction was calculated by image analysis software (Image J). Twenty fields were randomly selected under the microscope (×400) in cortex regions of each kidney sections for evaluation.

Immunohistochemical, immunofluorescence staining and frozen section

Kidney tissues were immersed in 4% paraformaldehyde and dehydrated by gradient alcohol, and then embedded in paraffin. After deparaffinization and hydration, 4 μm sections were treated for antigen reparation and incubated with indicated antibodies at 4 °C overnight followed by incubation with horseradish peroxidase-labeled secondary antibodies. Finally, slides were stained with hematoxylin.

H-score (3× percentage of strong staining + 2× percentage of moderate staining + percentage of weak staining, giving a range of 0–300) was used to quantify F4/80 and CD206 staining in mouse fibrotic renal. IHC antibodies: F4/80 (Cell Signaling Technology Cat# 70076, RRID: AB_2799771), CD206 (Cell Signaling Technology Cat# 24595, RRID: AB_2892682).

For immunofluorescence staining, kidney sections were stained with anti-LIF (R&D Systems Cat# AB-449-NA, RRID: AB_354362) and anti-FSP-1 (S100A4, Abcam Cat# ab197896, RRID: AB_2728774) at 4 °C overnight followed by incubating with corresponding AlexaFluor antibodies 1 h at room temperature, respectively. Nuclei were stained with DAPI. Images were taken by confocal microscopy (Olympus Corporation, Tokyo, Japan). At least 6 visual fields per section were analyzed for localization of cell markers.

Frozen-section slides of the kidney were made as soon as mice were sacrificed. Images were taken by fluorescence microscope (Olympus Corporation, Tokyo, Japan).

LIF ELISA

Concentrations of LIF in the tissue lysates of mice were measured using mouse-specific LIF ELISA kits (MLF00, R&D, Minneapolis, MN, USA) according to the manufacturer's protocols. The concentration of LIF in the culture medium of normal rat kidney interstitial fibroblast cell lines (NRK49F) was determined using rat-specific LIF ELISA kits (ELK5072, ELK Biotechnology, Wuhan, China).

Cell culture and treatment

Normal rat kidney tubular cell lines (NRK52E) were bought from American Type Culture Collection (ATCC, Gaithersburg, MD, Cat # CRL-1571, RRID: CVCL_0468) and NRK49F were kindly provided by Professor Youhua Liu (Departments of Pathology, and Medicine, University of Pittsburgh School of Medicine).[45,46] Cells were cultured in DMEM-Ham's medium (Gibco/Life Technologies, Grand Island, NY, USA) supplemented with 10% fetal bovine serum (FBS) (Gibco/Life Technologies, Grand Island, NY, USA). When 60% confluence was reached, cells were switched to serum-free medium for 12 h and treated with TGF-β1 (240-b-002, R&D, Minneapolis, MN, USA), TNF-α (T66674, Sigma–Aldrich, St. Louis, MO, USA), AngII (GF165, Sigma–Aldrich, St. Louis, MO, USA), SHH (HZ-1306, ProteinTech Group, Chicago, IL, USA), OSM (HY-P7052, MedChemExpress, NJ, USA), IL-11 (218-IL-005, R&D, Minneapolis, MN, USA) or LIF (7734-LF-025, R&D, Minneapolis, MN, USA) in the serum-free medium for indicated time period. In some experiments, cells were

Days after UIRI	6	7	8	9	10	11
Dosage of IgG or LIF-neutralizing antibody (mg/kg via the tail vein)	2	2	2.5	2.5	3	3

Table 6: **The dosage and time period of UIRI mice receiving IgG or LIF-neutralizing antibody.**

pretreated with indicated inhibitor for 30 min followed by incubation with vehicle or LIF for indicated time period. The inhibitors used were as follows: ERK inhibitor UO126 (#9903, Cell Signaling Technology, Beverly, Massachusetts, USA), STAT3 inhibitor stattic (s7024, Selleckchem, TX Houston, USA), hedgehog signaling pathway inhibitor cyclopamine (s1146, Selleckchem, TX Houston, USA). LIF used in cellular experiments was dissolved in PBS. Cell line validation and mycoplasma testing of NRK49F and NRK52E had been accomplished. All reagents were purchased from Guang Zhou Huajian Bioscience Co Ltd.

Isolation and culture of primary renal fibroblasts, renal tubular cells and bone marrow derived macrophages

Primary mouse renal fibroblasts were isolated as previously described.[47] Male C57BL/6 mice aged 8 weeks were euthanized by sodium pentobarbital, and kidneys were collected in the Clean Bench. Kidneys without capsules and renal pedicles were shredded and then washed with PBS until the tissues were white. Kidneys were digested with trypsin containing EDTA at 37 °C for 45 min, and then passed through 70 and 40 μm cell strainers. After centrifuging at 800 rpm for 5 min, the pellets were resuspended in DMEM/F-12 medium and centrifuged at 800 rpm for 5 min again. The cells were cultured in DMEM/F-12 medium containing 10% FBS in a humidified incubator.

Primary mouse proximal tubular epithelial cells (PTECs) were isolated as previously described.[48] Male C57BL/6 mice euthanized by sodium pentobarbital, and then kidneys were collected in a septic environment. The cortisol of the kidney was carefully separated and minced, and then washed with PBS until the tissues were white. The tissues were digested in 0.75 mg/ml collagenase Ⅳ (17104019, Gibco, Waltham, MA, USA) for 30 min at 37 °C. After centrifuging at 500 rpm for 2 min, those cells were washed with DMEM/F-12 medium by centrifuging at 500 rpm for 2 min. The tubular cells were isolated using 32% Percoll (17089101, Marlborough, MA, USA) gradients by centrifuging at 2000g at 4 °C for 10 min, and then resuspended with DMEM/F-12 medium. Primary tubular cells were cultured in DMEM/F-12 medium containing 10% FBS.

Bone marrow derived macrophages were isolated as previously described.[49] Briefly, fresh bone marrow (BM) cells were flushed out of the femur and tibia of the C57BL/6 mice with PBS buffer and cultured in RPMI Medium 1640 basic (Gibco) supplemented with 10% FBS in the presence of 10 ng/ml granulocyte macrophage colony-stimulating factor (GM-CSF, Peprotech). Fresh medium with 10% FBS and 10 ng/ml GM-CSF was added after 3 and 5 days. At day 7, the media were changed to RPMI Medium 1640 basic containing 1% FBS without GM-CSF 12 h before LIF (24 ng/ml, 24 h or 48 h) or vehicle treatments.

siRNA transfection

NRK49F cells and NRK52E cells were transfected with siEGR1 and siLIFR respectively using LipofectamineTM 2000 transfection reagent (Invitrogen, Carlsbad, CA, USA) according to the manufacturer's protocol, followed by treatment for different time period. The siEGR1 and siLIFR was purchased from RiboBio (Guangzhou, China). The RNA sequences of RNAi oligunucleotides were as follows:

EGR1-siRNA-1: 5′-GGACTTAAAGGCTCTTAAT-3′;
EGR1-siRNA-2: 5′-GGACAAGAAAGCAGACAAA-3′;
LIFR-siRNA-1:5′-TGAAATGCACAACCAACAA-3′;
LIFR-siRNA-2:5′-CATCGACTAGAGACAACAA-3′;

Cells counting

For counting cell numbers, NRK49F cells cultured in 12-well plate were digested with 200 μl trypsin containing EDTA (Gibco/Life Technologies, Grand Island, NY, USA) after treatment. The cell suspension was centrifuged at 800 rpm for 5 min and resuscitated the cells with PBS and equal 0.4% trypan blue staining solution (0418A19, Leagene Biotechnology, Beijing, China) to 1 ml. Cell numbers were counted by using a hemacytometer.

Bromodeoxyuridine (BrdU) incorporation assay

NRK49F cells were seeded onto 35 mm × 10 mm plates, and then pulsed with BrdU (10 mM) for 2 h. At the end of incubation, cells were fixed with 100% methanol followed by 0.2% Triton X-100 (1139ML100, Biofroxx, Einhausen, Germany) treatment. DNA was denatured by incubation with 2.5 N HCL for 1 h followed by neutralization with 0.1 M $NaHCO_3$. Cells were incubated diluted anti-BrdU (Abcam Cat# ab8152, RRID: AB_308713) antibody followed by incubating with Alexa Fluor® 594-conjugated goat anti-mouse IgG (invitrogen Cat# A-11005, RRID: AB_2534073). DAPI (ZLI-9557, Zsbio, Beijing, China) was added to stain the nuclei. The cells were observed with a fluorescence microscope (×100). Five randomly chosen microscopic fields were analyzed and the results are expressed as the cell proliferation rate calculated as follows: BrdU positive labeled cells/total number of cells ×100%.

Western blot analysis

Cells or kidney tissues were lysed with protein cracking liquid lysis buffer containing 0.1% protease inhibitor cocktail (Thermo Fisher, Rockford, IL, USA) for 30 min on ice. Lysates were subjected to Western blot analysis using the method described previously.[43] The following primary antibodies were used: anti-p-STAT2 (Abcam Cat# ab53132, RRID: AB_882712), anti-STAT2

(Abcam Cat# ab32367, RRID: AB_778098), anti-p-STAT4 (Abcam Cat# ab28815, RRID: AB_2196601), anti-STAT4 (Abcam Cat# ab55357, RRID: AB_882715), anti-p-STAT5a (Abcam Cat# ab30648, RRID: AB_779091), anti-p-STAT5a (Abcam Cat# ab128896, RRID: AB_11150987), anti-STAT5a (Abcam Cat# ab32043, RRID: AB_778107), anti-p-STAT5b (Abcam Cat# ab52211, RRID: AB_2196931), anti-STAT5b (Abcam Cat# ab178941, RRID: AB_2885102), anti-c-Myc (Abcam Cat# ab32072, RRID: AB_731658), anti-TNC (Abcam Cat# ab108930, RRID: AB_10865908), anti-a-SMA (Sigma–Aldrich Cat# A5228, RRID: AB_262054), anti-Fibronectin (Sigma–Aldrich Cat# F3648, RRID: AB_476976), anti-SHH (Sigma–Aldrich Cat# S8321, RRID: AB_1080054), anti-COL1A1 (Boster Biological Technology Cat# BA0325, RRID: AB_2891224), anti-LIF (Santa Cruz Biotechnology Cat# sc-515931, LOT# E0119) was purchased from UNIV, anti-p-ERK (Cell Signaling Technology Cat# 9101, RRID: AB_331646), anti-ERK (Cell Signaling Technology Cat# 4695, RRID: AB_390779), anti-p-JNK (Cell Signaling Technology Cat# 4668, RRID: AB_823588), anti-JNK (Cell Signaling Technology Cat# 9258, RRID: AB_2141027), anti-p-p38 (Cell Signaling Technology Cat# 9211, RRID: AB_331641), anti-p38 (Cell Signaling Technology Cat# 8690, RRID: AB_10999090), anti-Egr-1 (Cell Signaling Technology Cat# 4153, RRID: AB_2097038), anti-p-STAT1 (Cell Signaling Technology Cat# 7649, RRID: AB_10950970), anti-STAT1 (Cell Signaling Technology Cat# 14994, RRID: AB_2737027), anti-p-STAT3 (Cell Signaling Technology Cat# 9145, RRID: AB_2491009), anti-STAT3 (Cell Signaling Technology Cat# 4904, RRID: AB_331269), anti-Cyclin-D1 (Cell Signaling Technology Cat# 2978, RRID: AB_2259616), anti-GAPDH (Proteintech Cat# 60004-1-Ig, RRID: AB_2107436), anti-β-ACTIN (Proteintech Cat# 66009-1-Ig, RRID: AB_2687938) and anti-Tubulin (Proteintech Cat# 66240-1-Ig, RRID: AB_2881629).

Flow cytometry

Cells were gathered and suspended in FACS buffer. Fluorophore-conjugated antibodies were purchased from BioLegend (used at 1:100 dilution): FITC-F4/80 (123108, RRID: AB_893502), APC-CD86 (105012, RRID: AB_493342), Alexa Fluor 700-CD206 (141733, RRID: AB_2629636). FIXABLE VIABILITY DYE was purchased from Thermo Fisher (65-0865-14, used at 1:10000). Cells were dyed on ice, protected from light for 30 min, then centrifuged (1600 rpm/10 min), washed with FACS buffer and analyzed using an FACSCantoⅡ (BD Biosciences) flow cytometer.

Real-time PCR

Total RNA was isolated from NRK49F cells or kidney tissues with TRIzol (Vazyme Biotech Co, Ltd, Nanjing, China) reagent according to the manufacturer's instructions. Real-time PCR was performed on an ABI PRISM 7500 Fast sequence detection system (Applied Biosystems, Foster City, CA). The mRNA levels of indicated genes were calculated after normalizing with glyceraldehyde-3-phosphate dehydrogenase (GAPDH) by the comparative CT method ($2^{-\Delta\Delta Ct}$). The primers used in the experiments are listed in Table 7.

Statistical analysis

Categorical variables were presented as counts (percent) and continuous variables were presented as mean (SD). For continuous variates, comparisons between two groups were performed using Student's t test; comparisons among three or more groups were performed using one-way analysis of variance (ANOVA). If the differences among multi-groups were significant, Least-Significant Difference (LSD) test or Dunnett's T3 were used to analyze differences between each pair of groups. Spearman's coefficient correlation was used to assess the relationship between IL6 cytokines family expression and eGFR. Characteristics of the prospective CKD cohort were grouped and compared by reaching the renal endpoint or not. Complete data were collected and all patients were followed up during this cohort study. Cumulative kidney survival curves according to baseline uLIF levels (tertiles) were generated using the Kaplan–Meier method and compared using the log-rank test. Subgroup Kaplan–Meier analyses in patients with advanced CKD or overt proteinuria were also conducted. $P < 0.05$ was considered significant. RNA-seq data and patients' clinical indicators were analyzed by R 4.0.4 software. Animal and cell experiments data were analyzed by IBM SPSS software (version 21).

Role of funding source

The funders were not involved in study design, data collection, analysis, interpretation or writing of the manuscript.

Results

LIF is the most upregulated member of IL6 family in fibrotic kidneys of animal models

First of all, we systemically examined the expression of IL6 cytokines family in fibrotic renal tissues induced by IRI. As shown in Fig. 1a, although the mRNA level of *Cntf*, *Clcf1*, *Il6*, *Il11*, *Osm* and *Lif* were all significantly upregulated since day 3 after IRI, the level of *Lif* mRNA was the highest and the upregulation of *Lif* was sustained till day 14 after IRI. In mouse model of TIF induced by UUO, the expression of *Osm*, *Lif*, *Clcf1*, *Il11* and *Il6* was remarkably increased. *Lif* upregulation was most significant, and sustained till day 14 after UUO

Gene		Primer sequence (5′ to 3′)
Mouse *Gapdh*	Forward	GCACAGTCAAGGCCGAGAAT
Mouse *Gapdh*	Reverse	GCCTTCTCCATGGTGGTGAA
Mouse *Il31*	Forward	TCAGCAGACGAATCAATACAGC
Mouse *Il31*	Reverse	TCGCTCAACACTTTGACTTTCT
Mouse *Cd206(Mrc1)*	Forward	CTCTGTTCAGCTATTGGACGC
Mouse *Cd206(Mrc1)*	Reverse	CGGAATTTCTGGGATTCAGCTTC
Mouse *Arg1*	Forward	CTCCAAGCCAAAGTCCTTAGAG
Mouse *Arg1*	Reverse	AGGAGCTGTCATTAGGGACATC
Mouse *Shh*	Forward	AGATCACAAGAAACTCCGAACGA
Mouse *Shh*	Reverse	AACTTGTCTTTGCACCTCTGAGTC
Mouse *Il10*	Forward	GCTCTTACTGACTGGCATGAG
Mouse *Il10*	Reverse	CGCAGCTCTAGGAGCATGTG
Mouse *Lif*	Forward	AAAAGCTATGTGCGCCTAACA
Mouse *Lif*	Reverse	GTATGCGACCATCCGATACAG
Mouse *Il11*	Forward	TGTTCTCCTAACCCGATCCCT
Mouse *Il11*	Reverse	CAGGAAGCTGCAAAGATCCCA
Mouse *Kim-1(Havcr1)*	Forward	GTTAAACCAGAGATTCCCACACG
Mouse *Kim-1(Havcr1)*	Reverse	TCTCATGGGGACAAAATGTAGTG
Mouse *Cntf*	Forward	TCTGTAGCCGCTCTATCTGG
Mouse *Cntf*	Reverse	GGTACACCATCCACTGAGTCAA
Mouse *Clcf1*	Forward	GACTCGTGGGGGATGTTAGC
Mouse *Clcf1*	Reverse	CTAAGCTGCGGAGTTGATGCT
Mouse *Ctf1*	Forward	CCACCAGACTGACTCCTCAAT
Mouse *Ctf1*	Reverse	CTCCCTGTTGCTGCACGTA
Mouse *Tnf*	Forward	GCAAAGGGAGAGTGGTCA
Mouse *Tnf*	Reverse	CTGGCTCTGTGAGGAAGG
Mouse *Osm*	Forward	CCAGAGTACCAGGACCCA
Mouse *Osm*	Reverse	GCTGAGGAGCTGAGAGGA
Mouse *Il6*	Forward	AAAGAGTTGTGCAATGGCAATTCT
Mouse *Il6*	Reverse	AAGTGCATCATCGTTGTTCATACA
Mouse *Il27*	Forward	TGTCCACAGCTTTGCTGAAT
Mouse *Il27*	Reverse	GAAGTGTGGTAGCGAGGAAGC
Mouse *Ccl2*	Forward	CTTCTGGGCCTGCTGTTCA
Mouse *Ccl2*	Reverse	CCAGCCTACTCATTGGGATCA
Mouse *Il1β*	Forward	TGCCACCTTTTGACAGTGATG
Mouse *Il1β*	Reverse	AAGGTCCACGGGAAAGACAC
Mouse *Nos2*	Forward	GTTCTCAGCCCAACAATACAAGA
Mouse *Nos2*	Reverse	GTGGACGGGTCGATGTCAC
Mouse *Cxcl9*	Forward	TCCTTTTGGGCATCATCTTCC
Mouse *Cxcl9*	Reverse	TTTGTAGTGGATCGTGCCTCG
Mouse *Cxcl10*	Forward	CCAAGTGCTGCCGTCATTTTC
Mouse *Cxcl10*	Reverse	GGCTCGCAGGGATGATTTCAA
Rat *Gapdh*	Forward	TCCGCCCCTTCCGCTGATG
Rat *Gapdh*	Reverse	CACGGAAGGCCATGCCAGTGA
Rat *Tnf*	Forward	ATGGGCTCCCTCTCATCAGT
Rat *Tnf*	Reverse	GCTTGGTGGTTTGCTACGAC
Rat *Lif*	Forward	TCTTGGCCACAGGGATTGTG
Rat *Lif*	Reverse	TGTTGGGCGCACATAGCTTA
Rat *Il11*	Forward	AAAGACTCTGGAGCCAGAG
Rat *Il11*	Reverse	TAGGCGAGACATCAAGAGC
Rat *Gli1*	Forward	ATCCAATGACTTCACCACAAGT
Rat *Gli1*	Reverse	ATCCTAAAGAAGGGCTCATGGT
Rat *Il1β*	Forward	GAAGTCAAGACCAAAGTGG
Rat *Il1β*	Reverse	TGAAGTCAACTATGTCCCG
Rat *Ccl2*	Forward	TCTACAGAAGTGCTTGAGGTGGTTG
Rat *Ccl2*	Reverse	CCTGTTGTTCACAGTTGCTGCC

(Table 7 continues on next page)

Gene		Primer sequence (5′ to 3′)
(Continued from previous page)		
Rat *Il6*	Forward	CTCTCCGCAAGAGACTTCCAG
Rat *Il6*	Reverse	TGTGGGTGGTATCCTCTGTGA
Rat *Osm*	Forward	CCACCGAGAACACTGCTTAGTTTG
Rat *Osm*	Reverse	AGCCGAGCCATGCAGTAAAC
Rat *Cxcl14*	Forward	ATCCTAAGCTGCAAAGTACCA
Rat *Cxcl14*	Reverse	CCTACTCTTCGTAGACCCTG

Table 7: **Primers used in this study.**

(Fig. 1b). The expression of *Il31* was not detected in UUO or IRI model. Western blot analysis confirmed the elevated protein level of LIF in renal fibrotic lesions induced by both UUO and IRI (Fig. 1c–f). Meanwhile LIFR was also increased in these two models (Supplementary Fig. S1a–f). Consistent with our data, the most significant upregulation of *Lif* was detected in published RNA sequencing data (RNA-seq) (GSE98622, GSE118339)[31,32] (Supplementary Fig. S2a and b). Noteworthy, mass spectrometry analysis only detected the increased protein level of LIF in renal fibrotic lesion induced by UUO (GSE126182, Supplementary Fig. S2c).[32]

To explore the cellular sources of LIF in fibrotic kidney, we analyzed published single nucleus RNA sequencing (snRNA-seq) dataset of fibrotic kidney from mice 14 days after UUO.[39] LIF was mainly expressed in activated fibroblast 2, proliferating proximal tubule epithelial cells and collecting duct-principal cells (Fig. 1g). LIFR was ubiquitously expressed in variety of cells (Fig. 1h and j). We noticed that, similar to activated fibroblast 2, proliferating proximal tubule cells expressed mesenchymal marker "vimentin" as well as "PDGFD, SPP1, COL4a1", suggesting that proliferating proximal tubule cells exhibited the characteristics of mesenchymal cells.[39] Additionally, in a published Smart-Seq dataset of PDGFRβ$^+$ cells from mice 10 days after UUO, LIF was expressed in myofibroblasts, parietal epithelial cells and mesangial cells[40](Fig. 1i). To validate the scRNA-seq data, we conducted immunohistochemical staining in fibrotic kidney from mice 7 days after UUO. As shown in Fig. 1k, elevated LIF protein was predominantly detected in the tubulointerstitium. Dual immunofluorescence staining revealed the co-staining of LIF with FSP-1, a marker of fibroblasts (Fig. 1m). We did not observe obvious positive staining of LIF in renal tubular cells, probably because LIF is a secreted protein that is not easily detected as those intracellular proteins. Collectively, these data indicate that LIF was mainly expressed in activated fibroblasts in fibrotic renal lesions. In addition, immunohistochemical staining showed that LIFR was mainly detected in mesenchymal cells and some renal tubular cells (Fig. 1l).

LIF is upregulated and correlated with TIF and eGFR in patients with fibrotic kidney disease

In order to explore the relevance of LIF expression in the human TIF, we selected IgAN since the degree of TIF in IgAN could be calculated by Oxford MEST-T grade. The mRNA from renal biopsies of 33 IgAN patients were extracted for RNA-seq analysis. Six biopsy specimens from minimal change disease (MCD) patients were used as control. The clinical characters of patients were shown in Table 1. First of all, 39 patients were stratified into three groups according to the estimated glomerular filtration rate (eGFR): eGFR $\geq$ 90 (min/1.73 m^2); 89 (min/1.73 m^2) $\geq$ eGFR $\geq$ 60 (min/1.73 m^2); 59 (min/1.73 m^2) $\geq$ eGFR $\geq$ 30 (min/1.73 m^2). Among IL6 family members, only the *LIF* level was significantly increased along with the decline of eGFR (Fig. 2a; Supplementary Fig. S3a). Spearman's coefficient correlation revealed that, among IL6 family members, *LIF* showed the strongest correlation with eGFR with the smallest P value (r_s = –0.752, $P = 2.89 \times 10^{-7}$ by Spearman correlation) (Fig. 2b; Supplementary Fig. S3b). Next, we analyzed the association of TIF with the mRNA levels of IL6 family members in renal biopsies of IgAN patients. Compared with those MCD patients without TIF (n = 6), the mRNA level of *LIF* and *IL11* was significantly increased in patients with TIF, but the elevation of *LIF* (logFC = 1.128778, $P = 0.002333$ *vs* No TIF by R package limma) was higher than that of *IL11* (logFC = 0.644977, $P = 0.0245$ *vs* No TIF by R package limma) (Fig. 2c). Furthermore, among IL6 family members, only *LIF* level was significantly increased with the increase of Oxford MEST-T grade (Fig. 2d, Supplementary Fig. S3c), indicating that the elevation of *LIF* was associated with the severity of TIF.

We further confirmed the transcriptional changes of IL6 family members in other human CKD kidney specimens using the Nephroseq V5 transcriptomic database. We chose the ERCB Nephrotic Syndrome Data set which included RNA-seq data from 18 focal segmental glomerulosclerosis (FSGS), 10 diabetic nephropathy, and 9 healthy living donor samples. Differential analysis showed that, compared with healthy

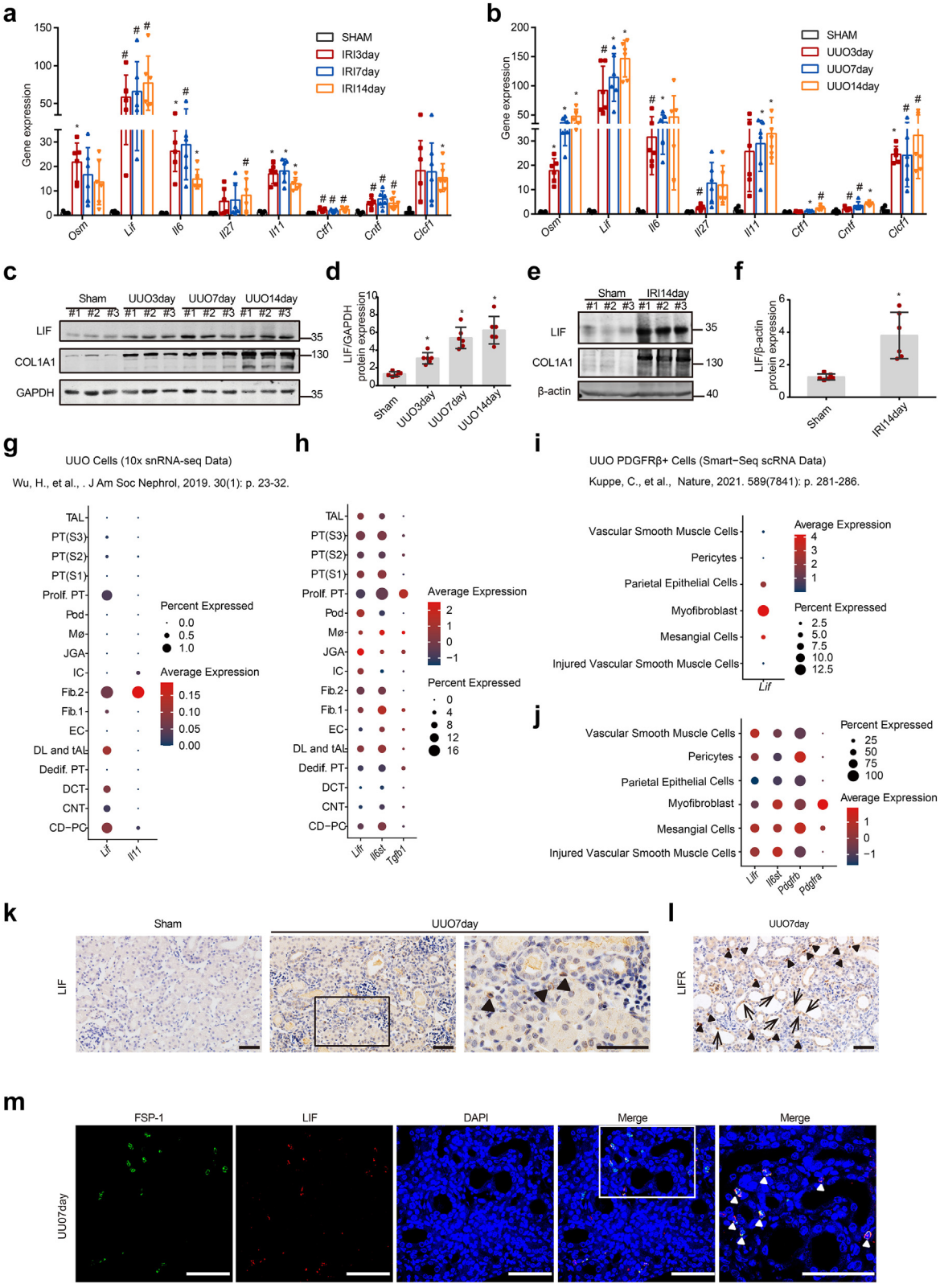

Fig. 1: **LIF was upregulated in fibroblasts in mouse models of TIF induced by UUO and IRI.** (a) The mRNA level of IL6 cytokines family at days 3, 7 and 14 after IRI (n = 6), normalized with gapdh. (b) The mRNA level of IL6 cytokines family at days 3, 7 and 14 after UUO (n = 6),

controls, only the levels of *LIF* (logFC = 1.051, $P = 0.01001$ *vs* No TIF by R package limma) and *CLCF1* (logFC = 0.764, $P = 0.00978$ *vs* No TIF by R package limma) were significantly increased in CKD samples. The level of *LIF* was higher than that of *CLCF1* (Fig. 2e). Both the levels of *LIF* ($r_s = -0.595$, $P = 3.37 \times 10^{-4}$ by Spearman correlation) and *CLCF1* ($r_s = -0.713$, $P = 6.45 \times 10^{-6}$ by Spearman correlation) were negatively correlated with eGFR (Fig. 2f, Supplementary Fig. S4). Collectively, these data indicate that LIF upregulation is a common feature of various human CKD.

Taupin et al.[50] reported the presence of LIF in the urine of kidney transplanted patients with acute rejection episodes, but not of those with stable renal function. Thus, we examined whether LIF protein can be detected in the urine of CKD patients. Western blotting showed that LIF protein in the urine of IgAN patients was readily detectable, but hardly visible in healthy volunteers (Fig. 2g). Next, the levels of LIF in the 24-h urine (uLIF) were measured by ELISA. The clinical characters of patients were shown in Tables 2 and 3. Compared with healthy controls, the uLIF level in IgAN patients was significantly increased. The uLIF level in IgAN patients was positively correlated with Oxford MEST-T stages, inversely correlated with renal function ($r_s = -0.624$, $P < 0.0001$ by Spearman correlation) (Fig. 2h and i). To investigate the relationship between uLIF and kidney outcome (end-stage kidney disease, ESRD) in CKD patients, we used bio-samples and data from a prospective cohort of Chinese patients with CKD (mean eGFR of 36 ml/min/1.73^2 and mean proteinuria of 2.2 g/d) with long-term follow-up. In this prospective cohort of CKD patients (N = 362, 59 cases of ESRD in a median 41 months follow-up), we found that baseline uLIF levels predicted the risk of CKD progression to ESRD (Fig. 2j). Furthermore, in subgroup analysis, baseline uLIF levels predicted the risk of CKD progression to ESRD both in patients with advanced CKD (eGFR < 60 ml/min/1.73 m^2; $P = 0.05$ by log-rank test; Fig. 2k) and overt proteinuria (≥1.0 g/d) ($P = 0.07$ by log-rank test; Fig. 2l), suggesting that higher expression of LIF might be a prominent indicator for TIF and disease progression in CKD.

LIF induces fibroblasts activation via ERK and STAT3 pathways

Since LIF was expressed in activated fibroblasts, we next explored the role of LIF in fibroblast activation. NRK49F cells were incubated with indicated concentration of recombinant human LIF. Cell counting revealed that LIF substantially increased the number of fibroblasts in a time- and dose-dependent manner (Fig. 3a). BrdU incorporation assay revealed increased BrdU incorporation in LIF-stimulated NRK49F cells (Fig. 3b and c). Consistently, proliferation-related proteins such as c-Myc, and Cyclin-D1 were induced by LIF in a dose-dependent manner (Fig. 3d and e). Moreover, LIF induced fibroblasts activation as manifested by the upregulation of α-smooth muscle actin (α-SMA), collagen1A1 (COL1A1), Fibronectin and tenascin-C (TNC) (Fig. 3d and e). Similar results were obtained when primary mouse renal fibroblasts were treated with various concentrations of recombinant human LIF (Supplementary Fig. S5a and b).

Next, we explored the pathways mediating the profibrotic effect of LIF. Western blotting showed that LIF increased the level of phosphorylated ERK (p-ERK), but not p38 and JNK, in a dose-dependent manner in NRK49F cells (Fig. 3f and g) and primary renal fibroblasts (Supplementary Fig. S5c and d). In addition, LIF significantly increased the level of phosphorylated STAT3 (p-STAT3) in NRK49F cells and primary renal fibroblasts with indicated concentrations of LIF (Fig. 3h and i and Supplementary Fig. S5e and f). U0126, the ERK pathway inhibitor, and Sttatic, the STAT3 inhibitor, remarkably blocked LIF-induced expression of c-Myc, Cyclin-D1, COL1A1, Fibronectin and TNC, as well as the inflammatory cytokines including *Ccl2*, *Il1β*, *Tnf*, and *Il11* but not *Il6* (Fig. 3j–l). Collectively, these data indicated that LIF induces fibroblasts activation and proliferation via ERK and STAT3 pathways.

normalized with gapdh. (c and d) Western blot analysis (c) and densitometric quantification (d) of LIF protein at days 3, 7 and 14 after UUO (n = 6). (e and f) Western blot analysis (e) and densitometric quantification (f) of LIF protein at day 14 after IRI (n = 6). (g) Dotplot illustrating expression of *Lif* and *Il11* in single nucleus RNA sequencing (snRNA-seq) dataset of fibrotic kidney from mice 14 days after UUO. (h) Dotplot illustrating expression of *Lifr*, *Il6st* and *Tgfb1* in single nucleus RNA sequencing (snRNA-seq) dataset of fibrotic kidney from mice 14 days after UUO. (i) Dotplot illustrating expression of *Lif* in a published Smart-Seq dataset of PDGFRβ$^+$ cells from mice 10 days after UUO. (j) Dotplot illustrating expression of *Lifr*, *Il6st*, *pdgfrb* and *pdgfra* in a published Smart-Seq dataset of PDGFRβ$^+$ cells from mice 10 days after UUO. (k) Representative LIF immunostaining in renal sections from sham mice (left panel) and UUO mice (middle and right panel). Magnification, ×400 (left and middle panel), ×1000 (right panel). Arrows indicate positive LIF expression. The boxed region was shown at higher magnification (right panels). Scale bar, 50 μm. (l) Representative LIFR immunostaining in renal sections from UUO 7 day mice. LIFR was detected in mesenchymal cells (Use triangle to indicate) and some tubular epithelial cells (Use arrows to indicate). Magnification, ×400. (m) Representative fluorescent images of coimmunostaining LIF (red) with FSP-1 (green) in renal sections from UUO mice. Arrows in magnified image indicate colocalization of LIF and FSP-1. The boxed region was showed at higher magnification. Scale bar, 50 μm. Data were expressed as means ± SD. $^{\#}P < 0.05$, $^{*}P < 0.01$ versus sham mice. *P* values were determined by Student's t-test in (f) and one-way ANOVA (Least-Significant Difference test or Dunnett's T3 test) in (a), (b) and (d). Data in (g) and (h) referenced frome Wu, H., et al., 2019. Data in (i) and (j) referenced frome Kuppe, C., et al., 2021.

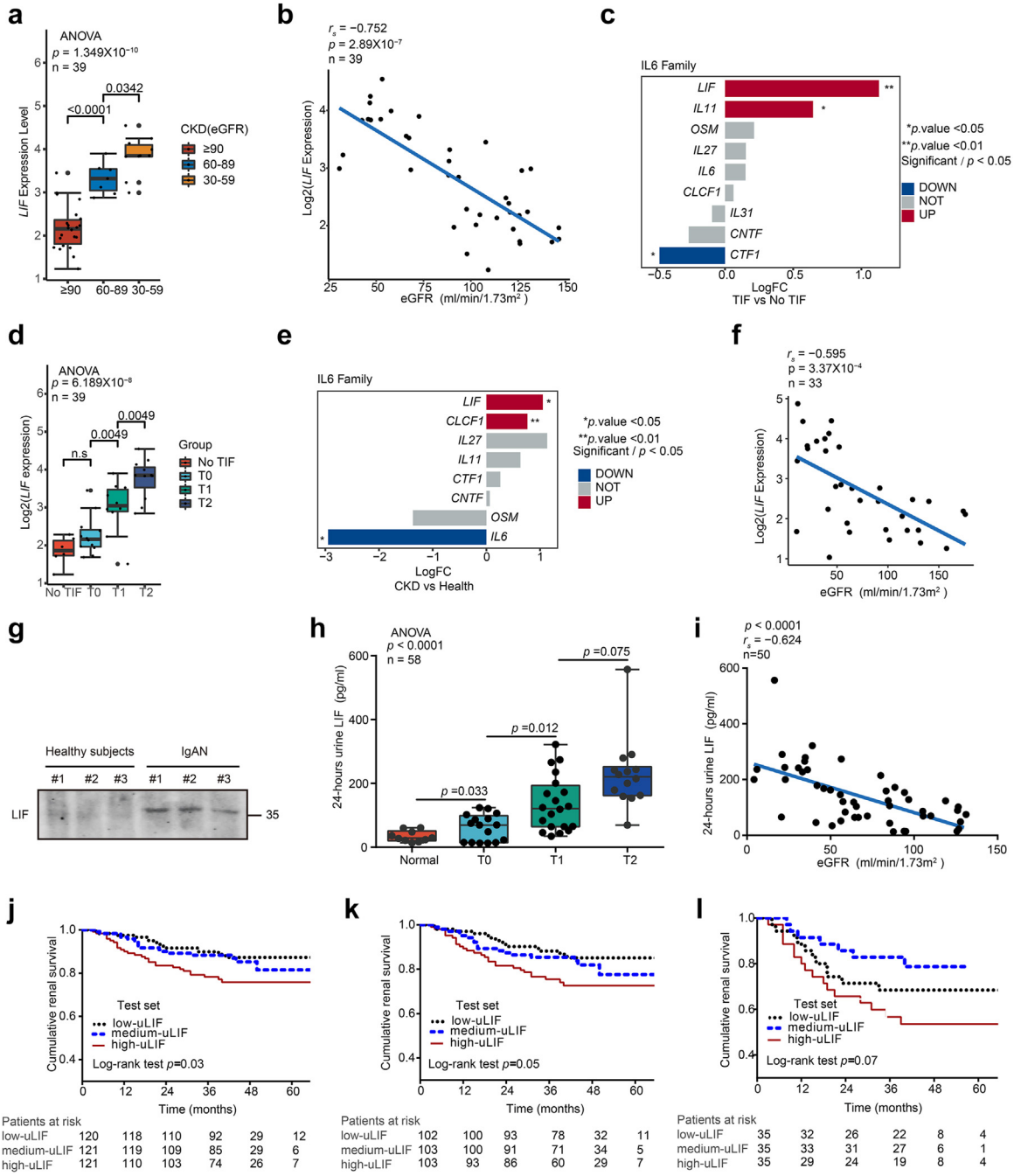

***Fig. 2:* LIF expression in renal biopsies and urine from CKD patients.** (a) The expression of LIF along with the decline of eGFR (n = 39). (b) The association between the log2 of LIF expression and eGFR (n = 39). (c) Differential expression of IL6 family cytokines between subjects with (n = 33) and without (n = 6) TIF. (d) The expression of LIF in different stages of Oxford-T grades of IgAN (n = 39). (e) Differential expression of IL6 family cytokines between CKD (n = 28) and healthy subjects (n = 9) from the ERCB Nephrotic Syndrome Data set. (f) The association between the log2 of LIF expression and eGFR in subjects (n = 33) from the ERCB Nephrotic Syndrome Data set. (g) Western blot analysis of LIF protein in 24 h-urine. (h) The amount of LIF protein in 24 h-urine was increased along with the stage of Oxford-T grades of IgAN (n = 50) and healthy controls (n = 8). The amount of LIF protein in 24 h-urine was measure by ELISA. (i) The amount of LIF protein in 24 h-urine negatively correlated with eGFR of IgAN patients (n = 50). (j–l) The level of uLIF at baseline predicts the risk of CKD progression to ESRD. Tertiles of uLIF-7 levels had a graded relationship with the risk of CKD progression to ESRD in total cohort (j), in subgroups of patients with eGFR <60 ml/min/1.73 m^2 (k) and patients with proteinuria >1.0 g/d (l). Data in (a), (d) and (h) were represented as median ± interquartile range (IQR) and *P* values were determined by one-way ANOVA (Least-Significant Difference test). The Spearman correlation analysis was used in (b), (f) and (i). The R package limma (3.46.0) was used in (c) and (e) for gene differential expression analysis between two groups. Data in (j), (k) and (l) were generated using the Kaplan–Meier method and compared using the log-rank test.

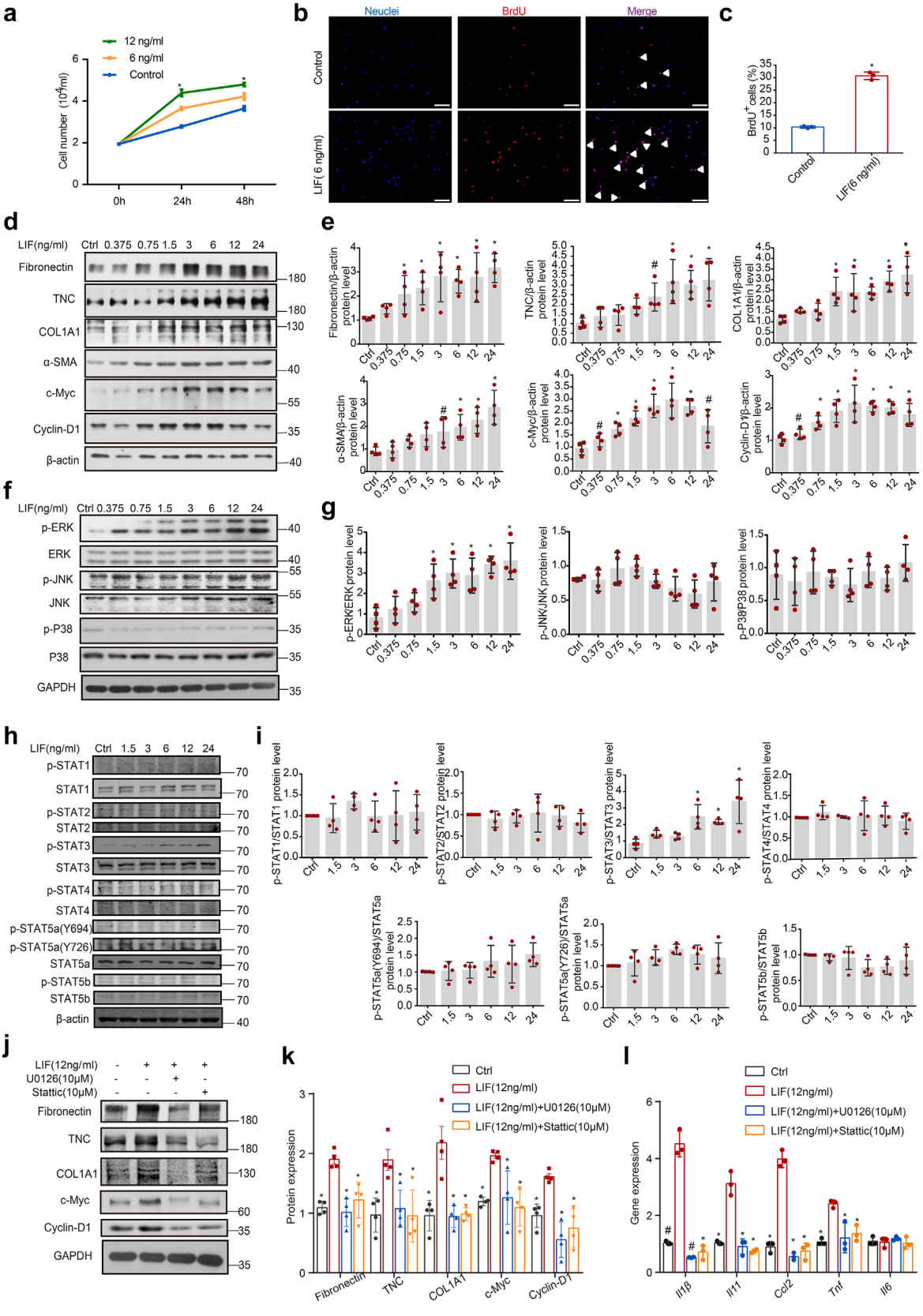
a
12 ng/ml
6 ng/ml
Control
Cell number (10⁴/ml)
0h
24h
48h
b
Neuclei
BrdU
Merge
Control
LIF(6 ng/ml)
c
BrdU+ cells (%)
Control
LIF(6 ng/ml)
d
LIF(ng/ml) Ctrl 0.375 0.75 1.5 3 6 12 24
Fibronectin
TNC
COL1A1
α-SMA
c-Myc
Cyclin-D1
β-actin
e
Fibronectin/β-actin protein level
TNC/β-actin protein level
COL1A1/β-actin protein level
α-SMA/β-actin protein level
c-Myc/β-actin protein level
Cyclin-D1/β-actin protein level
f
LIF(ng/ml) Ctrl 0.375 0.75 1.5 3 6 12 24
p-ERK
ERK
p-JNK
JNK
p-P38
P38
GAPDH
g
p-ERK/ERK protein level
p-JNK/JNK protein level
p-P38/P38 protein level
h
LIF(ng/ml) Ctrl 1.5 3 6 12 24
p-STAT1
STAT1
p-STAT2
STAT2
p-STAT3
STAT3
p-STAT4
STAT4
p-STAT5a(Y694)
p-STAT5a(Y726)
STAT5a
p-STAT5b
STAT5b
β-actin
i
p-STAT1/STAT1 protein level
p-STAT2/STAT2 protein level
p-STAT3/STAT3 protein level
p-STAT4/STAT4 protein level
p-STAT5a(Y694)/STAT5a protein level
p-STAT5a(Y726)/STAT5a protein level
p-STAT5b/STAT5b protein level
j
LIF(12ng/ml)
U0126(10μM)
Stattic(10μM)
Fibronectin
TNC
COL1A1
c-Myc
Cyclin-D1
GAPDH
k
Ctrl
LIF(12ng/ml)
LIF(12ng/ml)+U0126(10μM)
LIF(12ng/ml)+Stattic(10μM)
Protein expression
Fibronectin
TNC
COL1A1
c-Myc
Cyclin-D1
l
Ctrl
LIF(12ng/ml)
LIF(12ng/ml)+U0126(10μM)
LIF(12ng/ml)+Stattic(10μM)
Gene expression
Il1β
Il11
Ccl2
Tnf
Il6

LIF promotes pro-fibrotic response in renal tubular cells

Since LIFR was detected in renal tubular cells (Fig. 1l), we thus investigated whether LIF exerts any effect on renal tubular cells via RNA-seq analysis. GSVA analysis highlighted a number of pathways were up-regulated by LIF including SHH, JAK-STAT3, Notch and TGF-β1 signaling, whereas, fatty acid metabolism and oxidative phosphorylation were downregulated in LIF-treated cells (Fig. 4a). Western blotting revealed that LIF induced the protein level of α-SMA, Fibronectin, COL1A1, and TNC in primary renal tubular cells (Fig. 4b and c). These data indicated that LIF promotes pro-fibrotic response in renal tubular cells.

Renal tubule-derived SHH augments LIF expression in fibroblasts

Previous study showed that injured tubule-derived Sonic Hedgehog (SHH) activates fibroblasts,[51] suggesting that LIF-SHH signaling might mediate a crosstalk between fibroblasts and renal tubular cells. To address this issue, we validated LIF-upregulated SHH in primary renal tubular cells by real time PCR and western blotting (Fig. 5a–c). Previous studies reported that EGR1 is the downstream target of LIF-STAT3 signaling and ERK signaling.[52–57] Accordingly, depletion of LIFR or EGR1 by siRNA diminished LIF-augmented SHH expression, indicating that SHH is a downstream target of LIF-LIFR-EGR1 axis in renal tubular cells (Fig. 5d–g).

Next, we incubated NRK49F cells with SHH. Both mRNA and protein levels of LIF were elevated by SHH (Fig. 5h–j). Surprisingly, cyclopamine (CPN), an inhibitor of the canonical SHH pathway, did not block SHH-stimulated LIF expression. As the positive control, CPN abolished the expression of *Gli1*, a classic target gene of SHH (Supplementary Fig. S6), suggesting that SHH upregulates LIF expression via a non-canonical pathway. By searching Harmonizome database (https://maayanlab.cloud),[58] we found that EGR1 is a potential transcription factor regulating LIF expression. Western blotting revealed that SHH upregulated EGR1 expression in a dose-dependent manner (Fig. 5k and l). As expected, SHH-augmented LIF expression was dramatically inhibited when EGR1 was silenced by siRNA (Fig. 5m and n). Collectively, these data indicated that fibroblasts-derived LIF augment SHH expression in renal tubules. In turn, renal tubule-derived SHH augments LIF expression in fibroblasts and initiates fibroblasts activation. LIF-SHH signaling mediates a crosstalk between fibroblasts and renal tubular cells to boost pro-fibrotic response.

Upstream regulators of LIF expression in fibroblasts

Since EGR1 is the downstream target of ERK signaling and STAT3 signaling,[52–57] we sought LIF expression might be up-regulated by an autocrine pathway in fibroblasts. As expected, when NRK49F cells were incubated with indicated concentration of LIF for 24 h, both mRNA and protein level of LIF was increased in a dose-dependent manner (Fig. 6a–c). In addition, EGR1 was upregulated in a dose-dependent manner by LIF (Fig. 6b and c). When endogenous EGR1 was silenced by siRNA, LIF-augmented LIF expression was abolished (Fig. 6d and e). Since OSM could induce the expression of EGR1,[59,60] it might also upregulate LIF. Real-time PCR showed OSM, but not IL11, upregulate *Lif* in NRK49F (Fig. 6f). OSM also upregulated the expression of *Il11* and *Il6* in NRK49F but not NRK52E (Supplementary Fig. S7a and b). *Cxcl14* was used as a positive control.[61] Meanwhile LIF increased the expression of *Lif*, *Il11* and *Osm* (Supplementary Fig. S7c and d).

***Fig. 3:* LIF promoted proliferation, activation of rat fibroblasts through ERK1/2 and STAT3 pathway.** (a) NRK49F cells were incubated with LIF (6 ng/ml or 12 ng/ml) for 24 h or 48 h, and then cell numbers were counted. $^{\#}P < 0.05$, $^{*}P < 0.01$ versus controls (n = 3). (b and c) Representative micrographs of BrdU incorporation and quantitative determination of the percentage of BrdU-positive cells. Arrows indicate BrdU-positive cells. Scale bar, 100 μm. $^{\#}P < 0.05$, $^{*}P < 0.01$ versus controls (n = 3). (d and e) Western blot analyses (d) and quantitative data (e) showed that LIF upregulated the expression of proliferation and activation-related proteins in fibroblasts in a dose-dependent manner. NRK49F cells were incubated with indicated concentrations of LIF for 48 h. Cell lysates were subjected to Western blot analysis for c-Myc, Cyclin-D1, α-SMA, TNC, Fibronectin, and COL1A1. β-actin was used to verify equivalent loading. $^{\#}P < 0.05$, $^{*}P < 0.01$ versus controls (n = 4). (f and g) Representative Western blot (f) and quantitative data (g) showed that LIF induced phosphorylation of ERK1/2 in a dose-dependent manner. NRK49F cells were treated with indicated concentration of LIF for 30 min. $^{\#}P < 0.05$, $^{*}P < 0.01$ versus controls (n = 4). (h and i) NRK49F cells were treated with gradient concentration of LIF for 2 h. Representative Western blot (h) and quantitative data (i) showed that LIF induced phosphorylation of STAT3 in a dose-dependent manner. $^{\#}P < 0.05$, $^{*}P < 0.01$ versus controls (n = 4). (j and k) Representative Western blot (j) and quantitative data (k) showed that blockade of Mek1/ERK1/2 or STAT3 signaling abolished LIF-induced fibroblast proliferation and activation. NRK49F cells were pretreated with specific MEK1 and MEK2 inhibitor U0126 (10 μM) or STAT3 inhibitor stattic (10 μM) for 30 min followed by incubation with LIF (6 ng/ml) or vehicle for 24 h. Cell lysates were subjected to Western blot analyses for c-Myc, Cyclin-D1, TNC, Fibronectin, and COL1A1. $^{\#}P < 0.05$, $^{*}P < 0.01$ versus LIF alone (n = 4). (l) Real-time PCR analysis showed blockade of Mek1/ERK1/2 or STAT3 signaling reduced LIF-induced expression of pro-inflammatory cytokines in fibroblasts. NRK49F cells were pretreated with specific MEK1 and MEK2 inhibitor U0126 (10 μM) or STAT3 inhibitor stattic (10 μM) for 30 min, followed by incubation with LIF or vehicle for 24 h. Relative mRNA levels are reported after normalization with GAPDH. $^{\#}P < 0.05$, $^{*}P < 0.01$ versus LIF alone (n = 3). Data were expressed as means ± SD. *P* values were determined by Student's t-test in (c) or one-way ANOVA (Least-Significant Difference test or Dunnett's T3 test) in (a), (e), (g), (i), (k) and (l).

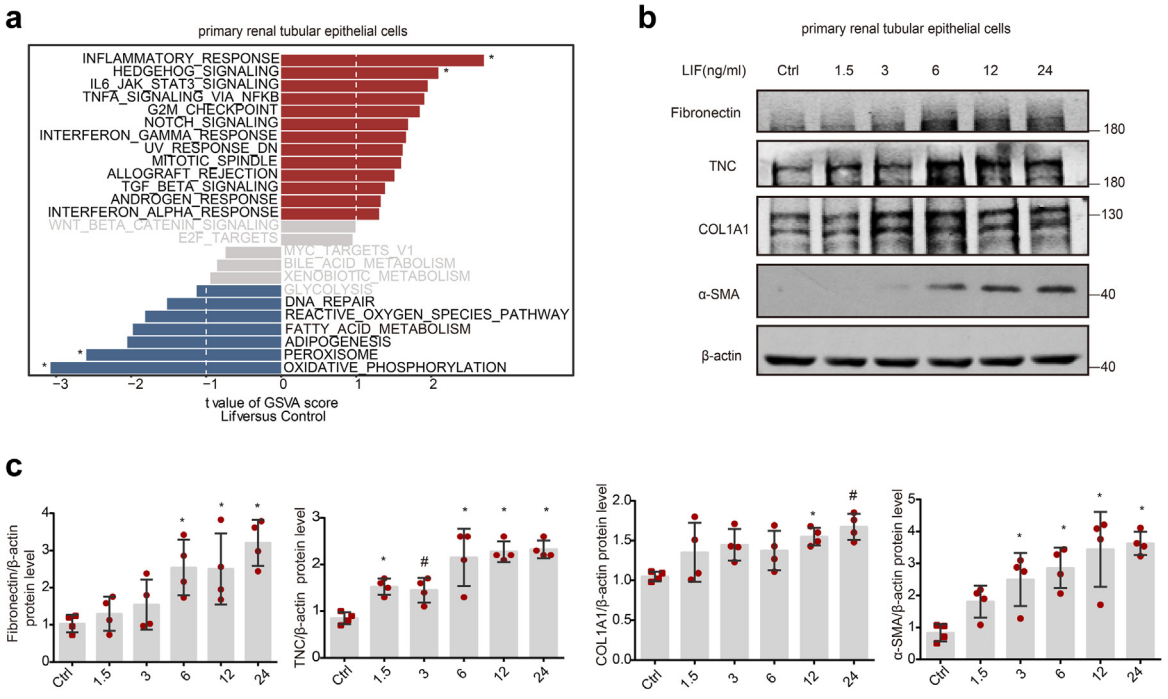

***Fig. 4:* LIF promotes pro-fibrotic response in renal tubular cells.** (a) Top enriched hallmark pathways identified by GSVA. The R package limma (3.46.0) was used for pathways differential expression analysis between two groups. (b and c) Representative Western blot (b) and quantitative data (c) showed LIF upregulated the expression of Fibronectin, TNC, COL1A1 and α-SMA in primary renal tubular epithelial cells in a dose-dependent manner. $^{\#}P < 0.05$, $^{*}P < 0.01$ versus controls (n = 4). One-way ANOVAs (Least-Significant Difference test or Dunnett's T3 test) in (c) was used for determining the *P* values while comparing between each pair of groups, respectively.

To further explore other upstream regulators of LIF expression, we stimulated NRK49F cells with a range of pro-fibrotic and pro-inflammatory factors. As shown in Fig. 6g, TNF-α, TGF-β1 and Angiotensin II (Ang II) upregulated *Lif* expression. Among them, TGF-β1 is the most powerful one. TGF-β1 increased the mRNA and protein level of LIF in a dose-dependent manner (Fig. 6h–j). ELISA revealed that TGF-β1 increased the concentration of LIF protein in the supernatant of NRK49F cells (Fig. 6k).

Ectopic expression of LIF aggregates TIF induced by UUO

To further investigate the potential fibrogenic role of LIF, we developed a lentivirus construct containing GFP-labeled LIF (lenti-GFP-LIF), and then injected it into renal parenchyma. Four days after injection, UUO was conducted and mice were sacrificed at days 7 post-UUO operation (Fig. 7a). The higher amount of LIF in lenti-GFP-LIF-injected kidneys was confirmed by frozen-section, real time PCR and western blotting (Fig. 7b–e). Masson trichrome and Sirius red staining showed that ectopic renal LIF expression augmented ECM deposition (Fig. 7f and g). Western blotting confirmed higher expression of α-SMA, COL1A1, TNC, Fibronectin, SHH and EGR1 (Fig. 7h and i) and heightened activation of STAT3 and ERK pathways (Fig. 7j and k). Real time-PCR showed that LIF over-expression enhanced UUO-induced expression of inflammatory cytokines such as *Ccl2*, *Tnf*, *Il11*, and *Il1β*, as well as *Kim-1* and *Shh* (Fig. 7l). Collectively, these data indicated that LIF overexpression exacerbated fibrotic lesion, inflammation and tubular cells injury induced by UUO.

Knockdown of LIFR ameliorates TIF induced by UUO

Next, we examined whether knockdown of LIFR affects the progression of TIF. LIFR was ubiquitously expressed in variety of cells (Fig. 1h and j). We therefore developed a lentivirus construct containing mouse LIFR-shRNA, and then injected it into renal parenchyma to wide-spread knock down LIFR in the kidney 4 days before UUO surgery (Fig. 8a). Knocking down LIFR dramatically decreased the mRNA and protein level of LIFR in UUO kidneys (Fig. 8b–d). Masson's trichrome and Sirius red staining indicated that knockdown of LIFR reduced interstitial ECM deposition induced by UUO (Fig. 8e and f). Western blot analyses confirmed the reduced protein level of TNC, Fibronectin, α-SMA, COL1A1, SHH, and EGR1 (Fig. 8g and h). Besides, the

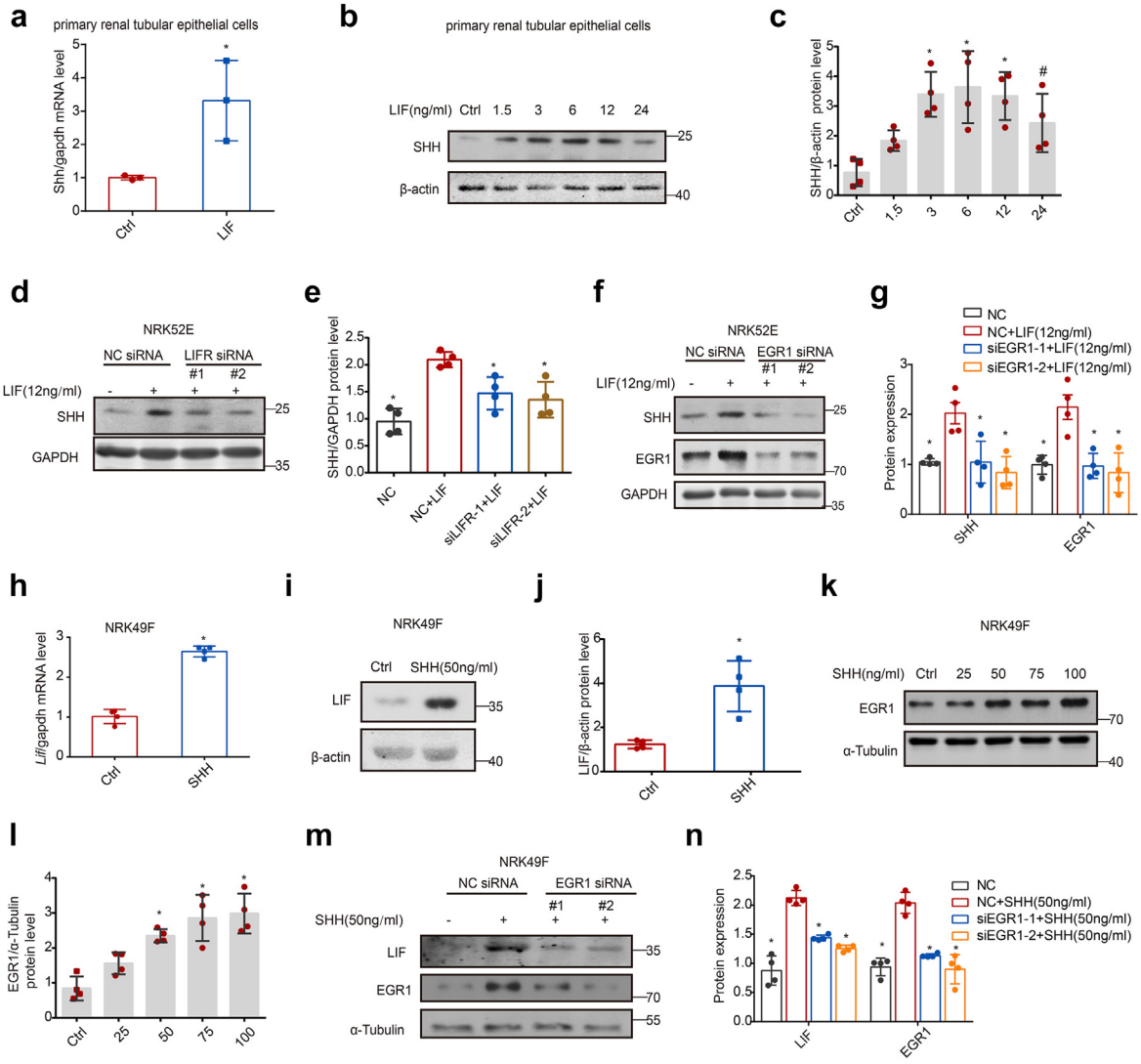

Fig. 5: **LIF and SHH mediated the crosstalk between fibroblasts and renal tubular cells.** (a) Quantitative real-time PCR showed the mRNA level of *Shh* induced by LIF (6 ng/ml, 24 h) in primary renal tubular epithelial cells, normalized with gapdh. **P* < 0.01 versus control (n = 3). (b and c) Representative Western blot (b) and quantitative data (c) showed LIF upregulated the expression of SHH in primary renal tubular epithelial cells in a dose-dependent manner. #*P* < 0.05, **P* < 0.01 versus controls (n = 4). (d and e) Representative Western blot (d) and quantitative data (e) showed silencing LIFR abolished LIF-induced SHH expression in NRK52E cells. NRK52E cells were transfected with scramble siRNA or siLIFR respectively, and then treated with 12 ng/ml LIF for 72 h. #*P* < 0.05, **P* < 0.01 versus scramble siRNA + LIF (n = 4). (f and g) Representative Western blot (f) and quantitative data (g) showed silencing EGR1 abolished LIF-induced SHH expression in NRK52E cells. NRK52E cells were transfected with scramble siRNA or siEGR1 respectively, and then treated with 12 ng/ml LIF for 72 h. (h) Quantitative real-time PCR showed that SHH (50 ng/ml, 24 h) upregulated the mRNA level of *Lif* in NRK49F cells. **P* < 0.01 versus control (n = 4). (i and j) Representative Western blot (i) and quantitative data (j) showed that SHH (50 ng/ml, 24 h) increased the protein level of LIF in NRK49F cells. **P* < 0.01 versus control (n = 4). (k and l) Western blot analyses (k) and quantitative data (l) showed the upregulation of EGR1 by SHH in NRK49F cells. **P* < 0.01 versus controls (n = 4). (m and n) Western blot (m) and quantitative data (n) showed SHH-induced LIF expression was attenuated by EGR1 siRNA. **P* < 0.01 versus LIF alone (n = 4). #*P* < 0.05, **P* < 0.01 versus scramble siRNA + LIF (n = 4). Data were expressed as means ± SD. Student's t-test in (a), (h) and (j) or one-way ANOVAs (Least-Significant Difference test or Dunnett's T3 test) in (c), (e), (g), (l) and (n) was used for determining the *P* values while comparing between each pair of groups, respectively.

levels of p-STAT3 and p-ERK were significantly decreased (Fig. 8i and j). As expected, the expression of *Il1β*, *Il11*, *Ccl2*, *Tnf* and *Lif* were significantly downregulated by LIFR knockdown (Fig. 8k). These results indicated that LIF-LIFR axis plays a pro-fibrotic role in TIF.

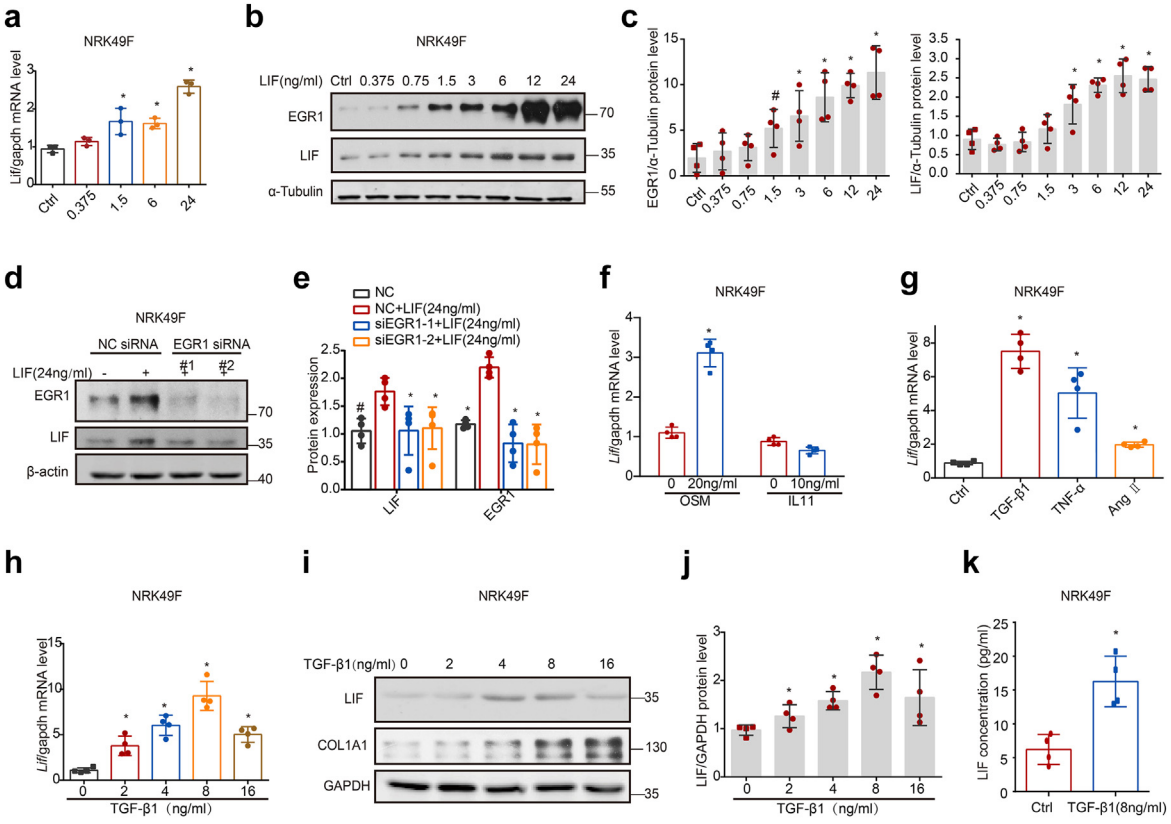

***Fig. 6:* Upstream regulators of LIF expression.** (a–e) LIF upregulated the expression of itself in NRK49F cells through ERK-EGR1 axis. NRK49F cells were treated with LIF for 24 h. (a) Real-time PCR showed that LIF upregulated itself in NRK49F cells. Relative *Lif* mRNA levels were shown as fold induction over controls after normalization with gapdh, respectively. $^{*}P < 0.01$ versus controls (n = 3). (b and c) Western blot analyses (b) and quantitative data (c) showed that LIF induced the expression of itself and EGR1 in a dose-dependent manner. $^{\#}P < 0.05$, $^{*}P < 0.01$ versus controls (n = 4). (d and e) Western blot analyses (d) and quantitative data (e) showed that knocking down EGR1 diminished LIF-induced LIF production. $^{\#}P < 0.05$, $^{*}P < 0.01$ versus NC+LIF (n = 4). (f) Upstream regulators of *Lif* expression. NRK49F cells were treated with OSM (20 ng/ml) and IL11 (10 ng/ml). (g) Upstream regulators of *Lif* expression. NRK49F cells were treated with TGF-β1 (8 ng/ml), TNF-α (8 ng/ml) and Ang II (10 nM/ml) for 24 h. Real-time PCR measured the mRNA level of *Lif*. Relative *Lif* mRNA levels were showed as fold induction over controls after normalization with gapdh, respectively. $^{*}P < 0.01$ versus controls (n = 4). (h) The mRNA level of *Lif* were induced by TGF-β1 induced LIF expression in a dose-dependent manner in NRK49F cells. $^{*}P < 0.01$ versus controls (n = 4). (i and j) Western blotting Representative Western blot (i) and quantitative data (j) showed that the protein level of LIF were induced by TGF-β1 in a dose-dependent manner in NRK49F cells. $^{\#}P < 0.05$, $^{*}P < 0.01$ versus controls (n = 4). (k) NRK49F cells were treated with TGF-β1 (8 ng/ml) for 24 h, and the LIF concentration in the culture medium was determined by ELISA. $^{*}P < 0.01$ versus controls (n = 4). Data were expressed as means ± SD. Student's t-test in (f), (g) and (k) or one-way ANOVAs (Least-Significant Difference test or Dunnett's T3 test) in (a), (c), (e), (h) and (j) was used for determining the *P* values while comparing between each pair of groups, respectively.

Therapeutic targeting LIF prevents TIF

We next investigated whether LIF in the kidney can be targeted therapeutically by a LIF-neutralizing antibody. Male BALB/C mice were subjected to UUO operation. To avoid acute-phase response, a LIF-neutralizing antibody was given via daily tail intravenous injection since day 3 after UUO (Fig. 9a). Masson's trichrome staining revealed that administration of LIF-neutralizing antibody dramatically reduced renal fibrotic lesions on day 14 after UUO (Fig. 9b and c). Western blot analyses confirmed reduced protein level of α-SMA, COL1A1, Fibronectin, TNC, EGR1 and SHH in LIF-neutralizing antibody-treated mice, together with attenuated activation of STAT3 and ERK pathways (Fig. 9d–g). In addition, UUO-induced expression of pro-inflammatory cytokines, including *Tnf*, *Ccl2*, *Il11* and *Il1β* was significantly inhibited by LIF-neutralizing antibody (Fig. 9h).

To further confirm the protective effect of LIF-neutralizing antibody on the progression of TIF, we constructed a different model of renal fibrosis induced by unilateral ischemia reperfusion injury (UIRI), which is more consistent with the clinical pathological process. Male C57BL/6 mice were subjected to UIRI. To avoid the acute phase effect, the LIF-neutralizing antibody was given via daily tail intravenous injection since day 6 after operation (Supplementary Fig. S8a). Serum creatinine

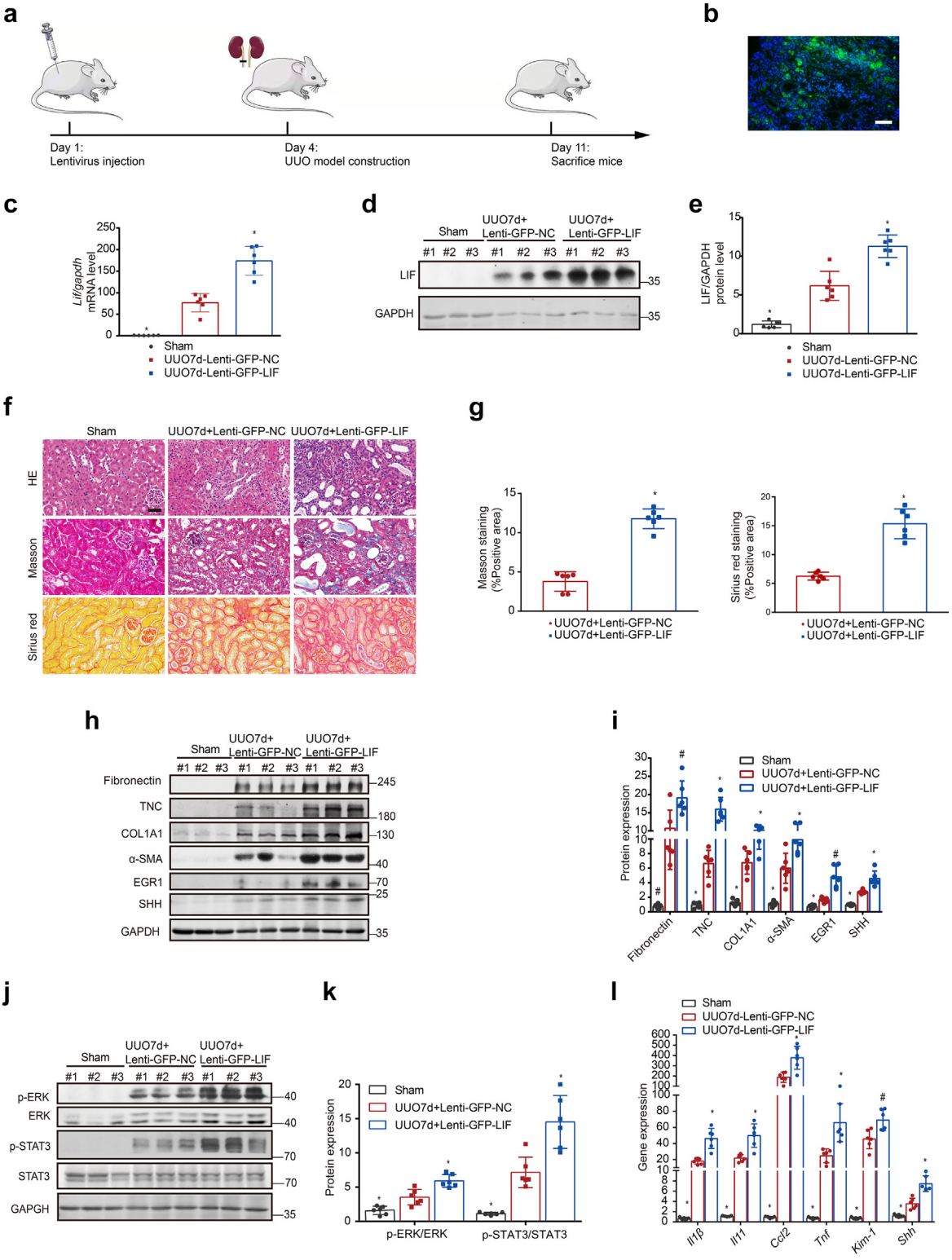

Fig. 7: **Ectopic expression of LIF exacerbated TIF induced by UUO.** (a) Schematic diagram showed the experimental design. (b) The frozen section of positive GFP-LIF staining at day 7 after UUO. Scale bar, 50 μm. (c) Real-time PCR showed the mRNA levels of *Lif* at day 7 after UUO. (d and e) The protein levels of LIF were assessed by Western blot at day 7 after UUO. Representative Western blot (d) and quantitative data (e) are

levels and Masson's trichrome staining revealed that anti-LIF treatment attenuated the decline of renal function, and reduced ECM deposition at 12 days after UIRI (Supplementary Fig. S8b–d). Consistent with histologic data, neutralization of LIF reduced the production of α-SMA, COL1A1, Fibronectin, TNC, EGR1 and SHH protein, together with reduced p-STAT3 and p-ERK (Supplementary Fig. S8e–h). Meanwhile, UIRI-induced expressions of *Tnf*, *Ccl2*, *Il11* and *Il1β* were diminished (Supplementary Fig. S8i).

LIF promoted macrophage infiltration and induced M2 macrophages polarization

Given the critical role of macrophages in the progression of renal fibrosis,[62] we tested whether LIF could influence infiltration and activation of macrophages. As shown in Fig. 10a, TGF-β1 significantly upregulated LIF expression in bone marrow-derived macrophages (BMDMs). On the other hand, when BMDMs were stimulated with LIF (24 ng/ml) for 48 h, LIF directly affects the polarization of macrophages to M2 phenotype, which is characterized by down-regulation of *Nos2*, *Cxcl10* and *Cxcl9* and up-regulation of *Arg1*, *Cd206* and *Il10* (Fig. 10b). Similarly, flow cytometry analysis showed increased percentage of CD206 positive macrophages and decreased percentage of CD86 positive macrophages (Fig. 10c and d). These data suggest that LIF promotes macrophage phenotype transition toward pro-fibrotic phenotype. Furthermore, we examined the infiltration of macrophages (F4/80) and M2 macrophages (CD206) in LIF-overexpressed UUO kidney by immunohistochemistry staining. The infiltration of macrophages and M2 macrophages were significantly increased (Fig. 10e and h). As expected, the infiltration of macrophages and M2 macrophages was decreased in mice treated with anti-LIF antibody (Fig. 10f, g and h).

Discussion

Accumulating literatures have reported the increased level of various IL6 family members, especially IL6, in the serum, urine or renal tissues of CKD patients. However, few have compared the expression of IL6 family members in the same cohort of patients. In the current study, we systemically evaluated the expression of all IL6 family members in both mouse and human fibrotic renal lesions. First of all, the expression of IL6 family members was examined in two preclinical animal models of TIF. To our surprise, LIF upregulation was most dramatic among IL6 family members. Furthermore, the highest expression of renal LIF was detected in various CKD biopsy specimens including IgAN, FSGS and diabetic nephropathy. The mRNA level of LIF significantly correlated with the decline of eGFR and the severity of TIF (Oxford MEST-T grade of IgAN). Importantly, in the prospective cohort, urinary LIF, measured at the time of baseline, predicted the risk of CKD progression to ESRD. These data, indicated that elevated LIF might play a pathogenic role in TIF. This hypothesis was further supported by the following experimental findings: ectopic expression of LIF in kidney aggregated TIF induced by UUO. While, knockdown of LIFR ameliorated TIF induced by UUO. Consistent with our finding, the pro-fibrotic effect of LIF has been reported in other organs. First, higher LIF expression was detected in myocyte of failing canine heart, and left ventricle of heart failure patients.[63,64] Heart-specific overexpression of LIF caused cardiac hypertrophy.[65] Second, transgenic mice expressing LIF from the insulin promoter displayed considerable interstitial fibrosis throughout the pancreas.[66,67] However, in the case of TIF, the results are still controversial. Matsumto et al.[68] reported that subcapsular administration of LIF did not obviously affect the degree of TIF in both UUO and folic acid nephropathy models. To address this difference, we measured the concentration of LIF in the fibrotic renal tissues by ELISA. The concentration of LIF was around 890 pg/ml on day 7 after UUO (Supplementary Fig. S9). Whereas, the amount of LIF administrated by Matsumoto et al. was 100 pg/kidney, which might not be enough to achieve any obvious effect. On the other hand, LIF is reported to promote tubular regeneration after acute kidney injury (AKI).[69] We analyzed the published snRNA-seq dataset of fibrotic kidney from mice 14 days after UUO,[39] and found that LIF expressed in proliferous proximal tubular cells (Fig. 1g), suggesting that LIF might be implicated in renal tubular proliferation after renal injury. To explore the possible mechanism, we analyzed bulk RNA-seq data of LIF-treated primary PTECs. Compared with control, both Rspo3, an exocrine protein activating canonical Wnt signaling,[70] and Wnt 10 were significantly upregulated by LIF (Supplementary Fig. S10).

showed. (f and g) Representative images of H&E, Masson trichrome and Sirius red staining of renal cortex at day 7 after UUO in three groups (f) and quantitative analysis of fibrotic area (g). Scale bar, 50 μm. (h and i) Western blotting showed the protein levels of TNC, Fibronectin, COL1A1, α-SMA, EGR1, SHH at day 7 after UUO. Representative Western blot (h) and quantitative data (i) are showed. (j and k) The protein levels of p-ERK, ERK, p-STAT3 and STAT3 were assessed by Western blot analyses at day 7 after UUO. Representative Western blot (j) and quantitative data (k) are showed. (l) Real-time PCR showed the mRNA levels of *Il1β*, *Il11*, *Ccl2*, *Tnf*, *Kim-1* and *Shh* at day 7 after UUO. Data were expressed as means ± SD. Student's t-test in (g) or one-way ANOVAs (Least-Significant Difference test or Dunnett's T3 test) in (c), (e), (i), (k) and (l) was used for determining the *P* values while comparing between each pair of groups, respectively, $^{\#}P < 0.05$, $^{*}P < 0.01$ versus UUO 7day-lenti-GFP-NC (n = 6).

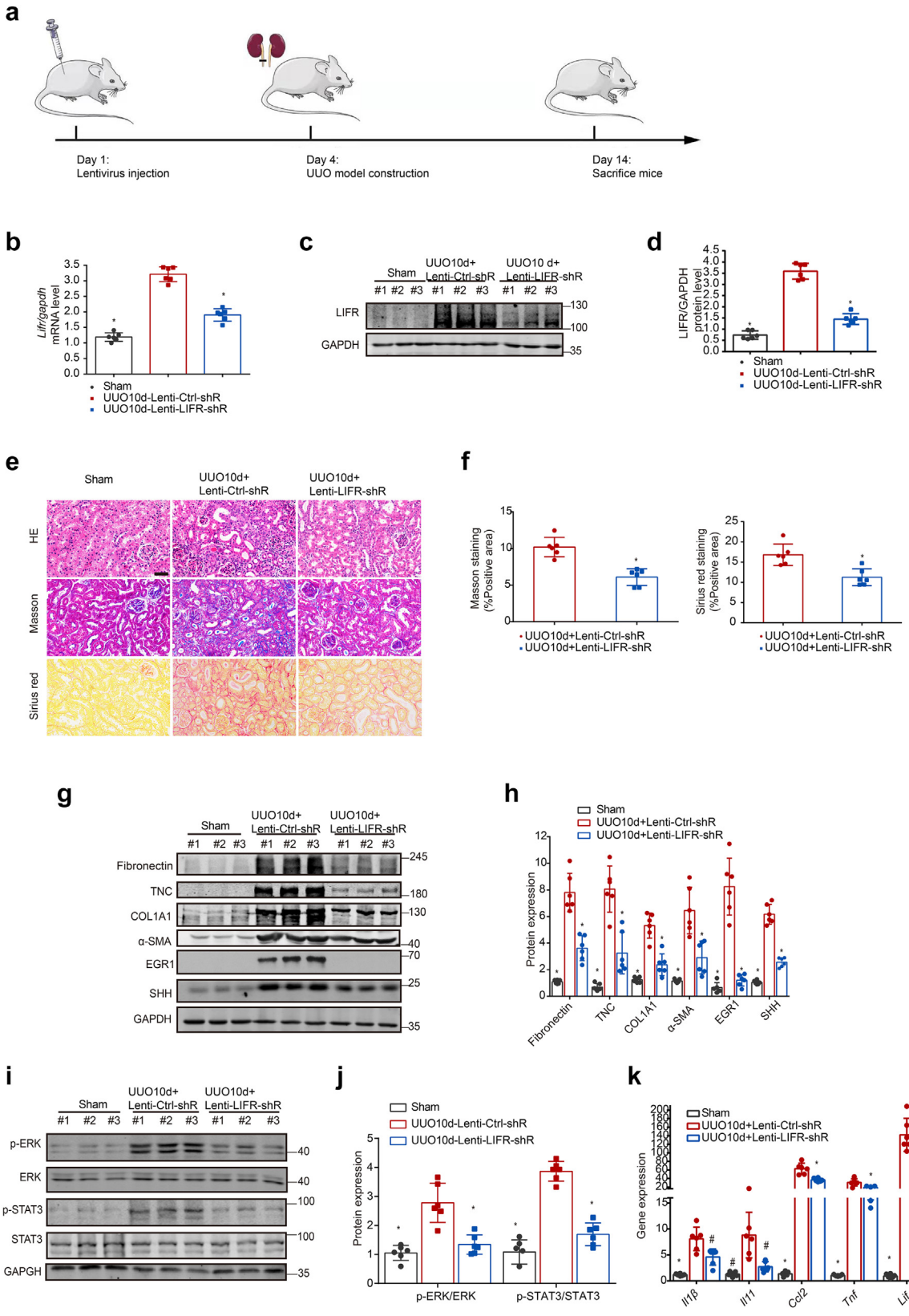
a
Day 1:
Lentivirus injection
Day 4:
UUO model construction
Day 14:
Sacrifice mice
b
Lifr/gapdh mRNA level
Sham
UUO10d-Lenti-Ctrl-shR
UUO10d-Lenti-LIFR-shR
c
Sham
UUO10d+ Lenti-Ctrl-shR
UUO10 d+ Lenti-LIFR-shR
#1 #2 #3 #1 #2 #3 #1 #2 #3
LIFR
GAPDH
130
100
35
d
LIFR/GAPDH protein level
Sham
UUO10d-Lenti-Ctrl-shR
UUO10d-Lenti-LIFR-shR
e
Sham
UUO10d+ Lenti-Ctrl-shR
UUO10d+ Lenti-LIFR-shR
HE
Masson
Sirius red
f
Masson staining (%Positive area)
Sirius red staining (%Positive area)
UUO10d+Lenti-Ctrl-shR
UUO10d+Lenti-LIFR-shR
g
Sham
UUO10d+ Lenti-Ctrl-shR
UUO10d+ Lenti-LIFR-shR
#1 #2 #3 #1 #2 #3 #1 #2 #3
Fibronectin
TNC
COL1A1
α-SMA
EGR1
SHH
GAPDH
245
180
130
40
70
25
35
h
Sham
UUO10d+Lenti-Ctrl-shR
UUO10d+Lenti-LIFR-shR
Protein expression
Fibronectin
TNC
COL1A1
α-SMA
EGR1
SHH
i
Sham
UUO10d+ Lenti-Ctrl-shR
UUO10d+ Lenti-LIFR-shR
#1 #2 #3 #1 #2 #3 #1 #2 #3
p-ERK
ERK
p-STAT3
STAT3
GAPGH
40
40
100
100
35
j
Sham
UUO10d-Lenti-Ctrl-shR
UUO10d-Lenti-LIFR-shR
Protein expression
p-ERK/ERK
p-STAT3/STAT3
k
Sham
UUO10d+Lenti-Ctrl-shR
UUO10d+Lenti-LIFR-shR
Gene expression
Il1β
Il11
Ccl2
Tnf
Lif

Since Wnt signaling promotes renal tubular cells proliferation during acute kidney injury (AKI), it is possible that LIF modulated Rspo 3 expression to activate Wnt signaling and promote injured tubular epithelial cells proliferation during AKI. However, sustained activation of Wnt signaling contributes to the pathogenesis of renal fibrosis.[71,72] Yu et al.[73] reported attenuated TIF in mice given LIF since day 1 after UUO. Since LIF promotes tubular regeneration after AKI, administration of LIF on Day 1 might attenuate acute renal tubular injury leading to reduced TIF later. In the current study, to avoid acute-phase response, a LIF-neutralizing antibody was given since day 3 after UUO, and attenuated TIF was observed on day 14 after UUO. Similarly, to avoid the increase of LIF during acute phase of UUO operation, we chose lentivirus system to overexpress LIF in renal parenchyma since the gene delivered by lentivirus could be slightly detected on day 3 and reach the peak level on day 7 after infection.[74] It was noteworthy that the expression of protein lags behind the gene expression. Collectively, these data indicate that LIF plays a pro-fibrotic role in the progression of TIF. Noteworthy, LIF is upregulated in human diabetic nephropathies and FSGS (Fig. 2e). Meanwhile LIFR is expressed in mesangial cells and parietal epithelial cells in glomeruli (Fig. 1j). Previous study showed that high-glucose induces LIF expression in human mesangial cells,[75] and activation of STAT3 signaling contributes to high-glucose-mediated cell growth, and fibronectin synthesis in mesangial cells.[76] Thus, it is possible that LIF is involved in high glucose induced mesangial cell activation via activating STAT and MAPK pathways. Moreover, it has been showed that LIF upregulated the expression of MCP-1 in mesangial cells to promote glomerular inflammation.[77] Transgenic mice overexpressing LIF in T lymphocytes displayed mesangial proliferative glomerulonephritis.[78] These data suggest that persistently elevated LIF might also contribute to the pathogenesis of glomerulosclerosis.

To explored the mechanisms driving the excess production of LIF, we found EGR1 as a potential transcription factor regulating LIF expression by searching Harmonizome database. Furthermore, we demonstrated that a positive feedback loop involving autocrine LIF, LIFR, and EGR1 drives sustained LIF transcription in fibroblasts. Consistent with previous report that EGR1 is a downstream target of TGF-β1, we demonstrated that TGF-β1 potently upregulated LIF expression in both fibroblasts and macrophages. Besides TGF-β1, a variety of pro-fibrotic stimuli implicated in CKD including hypoxia, oxidative stress, and PDGF, are potent inducers of EGR1 expression,[79,80] and might also contribute to the persistent LIF upregulation in the micro-environment of fibrotic lesions. On the other hand, we showed that LIF upregulated EGR1 expression via LIFR-ERK axis. Given the critical role of EGR1 in the extracellular matrix production, ROS generation, and the production of various fibrogenic growth factors and cytokines,[79,81–83] elevated EGR1 expression might at least partially mediate the pro-fibrotic role of LIF.

Regarding to the mechanism by which LIF promoted TIF, we provided evidence that LIF activated fibroblasts via ERK and STAT3 pathway. Second, since LIFR is expressed in renal tubular cells, we demonstrated that LIF induced pro-fibrotic response of renal tubular cells via activating a couple of signalings including SHH, JAK-STAT3, Notch and TGF-β1 signaling. In turn, tubule-derived Shh further upregulated LIF expression in fibroblasts. Based on the above data, we concluded that LIF-Shh mediates a crosstalk between fibroblasts and renal tubular cells to augment the LIF expression and the pro-fibrotic response of both fibroblasts and renal tubular cells. In addition, LIF significantly upregulated OSM expression in both NRK49F and NRK52E cells (Supplementary Fig. S7c and d), and OSM upregulated LIF expression in NRK49F cells (Fig. 6f), suggesting that, in fibrotic renal lesion, LIF and OSM forms another vicious cycle between renal tubular cells and fibroblasts to accelerate fibrosis progression. Besides, LIF upregulates IL11 expression in renal fibroblasts (Supplementary Figure 7c), suggesting that upregulation of IL11 and OSM also contributes to the pro-fibrotic role of LIF in TIF. Together with previous finding that OSM upregulates IL11 expression in cardiac fibroblasts[21] and LIF upregulates IL11 in synovial fibroblasts,[84] OSM, LIF and IL11 might play a critical role in organ fibrosis.

There are limitations in our study. To evaluate the pro-fibrotic role of LIF, transgenic mice or knockout mice could provide more convincing evidence. However, LIFR deficient mice die perinatally due to pleiotropic defects including urinary tract malformations.[85] Second, specific depleting LIFR in renal tubules or fibroblasts might not

***Fig. 8:* Knocking down LIFR ameliorated renal fibrotic lesions induced by UUO.** (a) Schematic diagram of the experimental design. (b) Real-time PCR showed the mRNA levels of *Lifr* at day 10 after UUO. (c and d) Representative Western blot (c) and quantitative data (d) showed the protein level of LIFR at day 10 after UUO. (e and f) Representative images of H&E, Masson trichrome and Sirius red staining of renal cortex at day 10 after UUO in three groups (e) and quantitative analyses of fibrotic area (f). Scale bar, 50 μm. (g and h) Representative Western blot (g) and quantitative data (h) showed the protein levels of TNC, Fibronectin, COL1A1, α-SMA, EGR1, SHH at day 10 after UUO. (i and j) Representative Western blot (i) and quantitative data (j) showed the protein levels of p-ERK, ERK, p-STAT3 and STAT3 at day 10 after UUO. (k) Real-time PCR showed the mRNA ± levels of *Il1β*, *Il11*, *Ccl2*, *Tnf* and *Lif* at day 10 after UUO. Data were expressed as means ± SD. Student's t-test in (f) or one-way ANOVAs (Least-Significant Difference test or Dunnett's T3 test) in (b), (d), (h), (j) and (k) was used for determining the *P* values while comparing between each pair of groups, respectively, $^{\#}P < 0.05$, $^{*}P < 0.01$ versus UUO10day+Lenti-Ctrl-shR (n = 6).

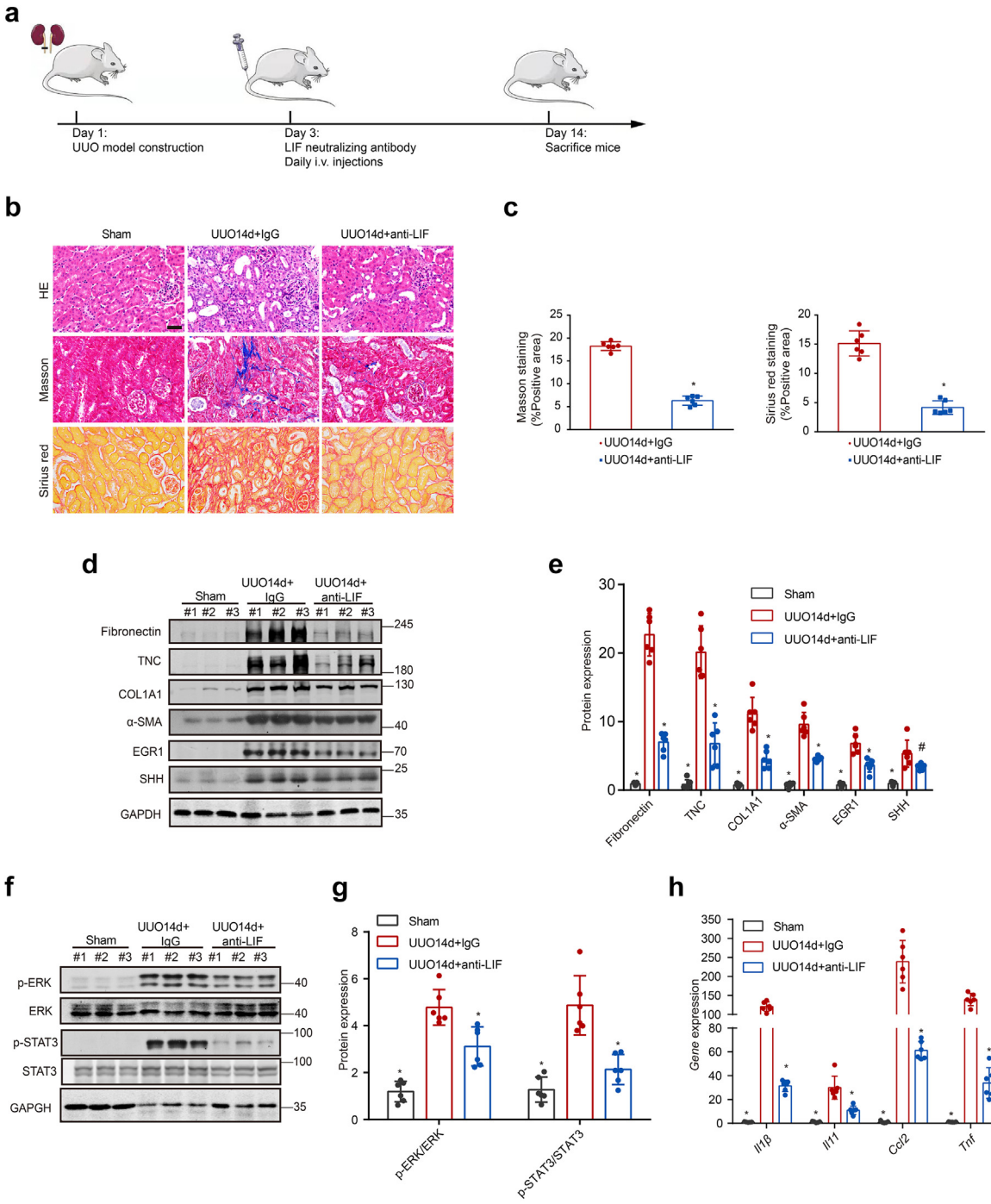

Fig. 9: **Neutralizing LIF antibody attenuated renal fibrosis induced by UUO.** (a) Schematic diagram of the experimental design. (b and c) Representative images of H&E, Masson trichrome and Sirius red staining of renal cortex at day 14 after UUO in three groups (b) and quantitative analyses of fibrotic area (c). Scale bar, 50 μm. (d and e) Representative Western blot (d) and quantitative data (e) showed the protein levels of TNC, Fibronectin, COL1A1, α-SMA, EGR1and SHH at day 14 after UUO. (f and g) Representative Western blot (f) and quantitative data (g) showed the protein levels of p-ERK, ERK, p-STAT3 and STAT3 at day 14 after UUO. (h) Real-time PCR showed the mRNA levels of *Il1β*, *Il11*, *Ccl2* and *Tnf* at day 14 after UUO. Data were expressed as means ± SD. Student's t-test in (c) or one-way ANOVAs (Least-Significant Difference test or Dunnett's T3 test) in (e), (g) and (h) was used for determining the *P* values while comparing between each pair of groups, respectively, $^{\#}P < 0.05$, $^{*}P < 0.01$ versus UUO14day-IgG (n = 6).

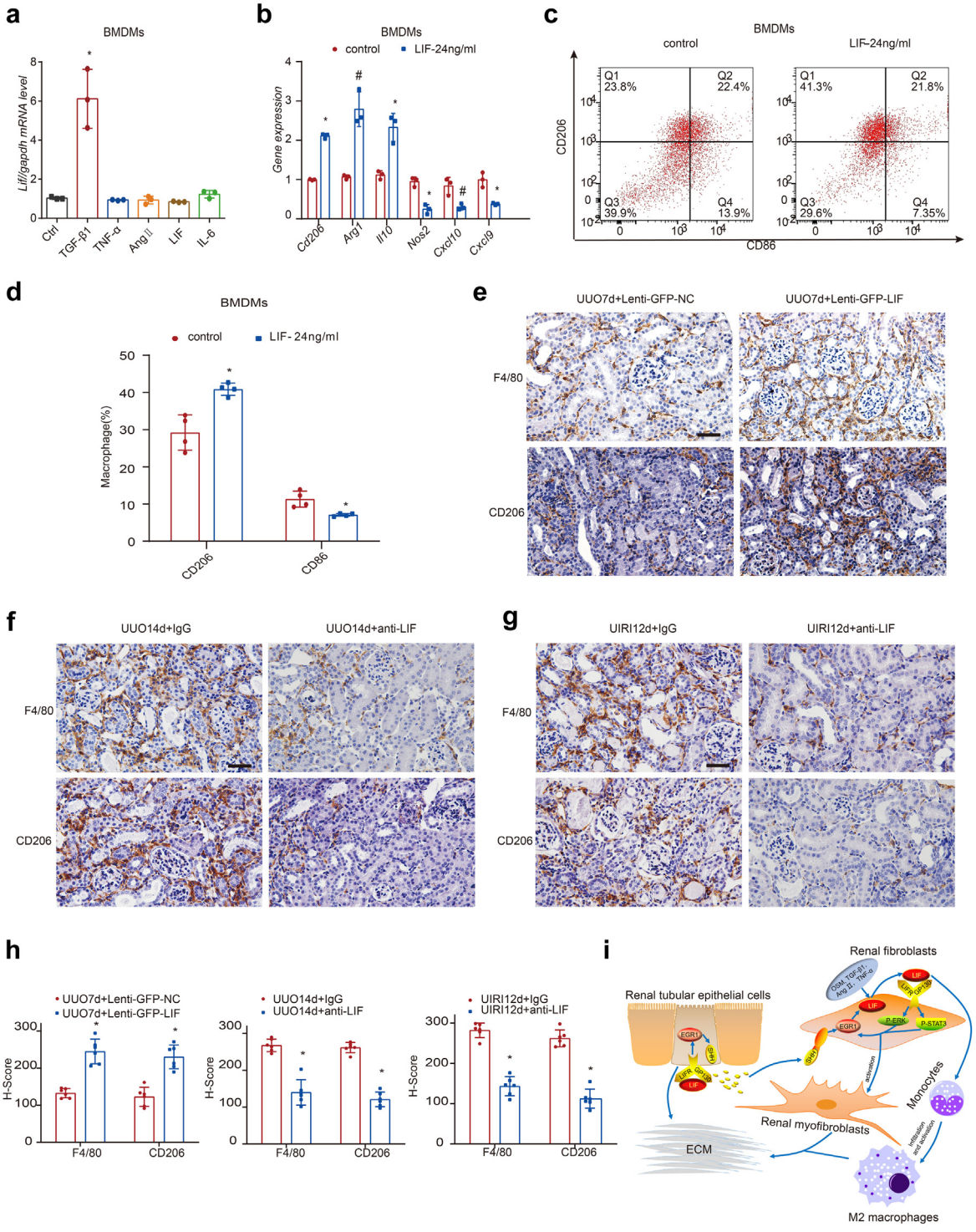

***Fig. 10*: LIF promoted macrophage infiltration and induced M2 macrophages polarization.** (a) BMDMs were treated with TGF-β1 (8 ng/ml), TNF-α (8 ng/ml), Ang II (10 nM/ml), LIF (24 ng/ml) and IL6 (10 ng/ml) for 24 h. $^{\#}P < 0.05$, $^{*}P < 0.01$ versus controls (n = 3). (b) BMDMs were treated with LIF for 48 h. Real-time PCR measured the mRNA level of *Cd206*, *Arg1*, *Il10*, *Nos2*, *Cxcl10* and *Cxcl9*. Relative mRNA levels were showed as fold induction over controls after normalization with gapdh, respectively. $^{\#}P < 0.05$, $^{*}P < 0.01$ versus controls (n = 3). (c and d) Flow cytometry analysis of BMDMs polarization with or without LIF stimulation (c) and quantitative data (d). $^{\#}P < 0.05$, $^{*}P < 0.01$ versus controls (n = 4). (e) Representative F4/80 and CD206 IHC image at day 7 after UUO in two groups. (f and g) Representative F4/80 and CD206 IHC image

be able to reduce TIF significantly since LIFR is broadly expressed in variety of cells. Third, LIF knockout mice showed neurological and endocrine system abnormalities.[86,87] In addition, since LIF is involved in kidney development,[88] certain renal cell-specific LIF knockout might display kidney developmental defect. Based on the above reasons, we chose to inject LIFR-shRNA lentivirus into renal parenchyma to block the pro-fibrotic effect of LIF in vivo. To evaluate the effect of LIF overexpression on TIF, we injected lenti-GFP-LIF lentivirus to increase LIF concentration in renal parenchyma of UUO mice. In the future, fibroblast-specific LIF transgenic mice would be necessary to evaluate whether LIF overexpression could directly induce TIF in normal kidneys. Finally, in the prospective cohort of CKD patients (N = 362), we found that baseline uLIF levels could predict the risk of CKD progression to ESRD. However, the *P* value was barely statistically different ($P = 0.07$ by log-rank test) in patients with overt proteinuria (≥1.0 g/d) because the sample size of CKD patients with overt proteinuria in our cohort is relatively small (n = 105, 35 patients per tertile of uLIF). Future larger prospective cohort study in patients with overt proteinuria and longer follow up is warrant. In addition, our prospective study population was Chinese. Further studies are needed to investigate whether uLIF could predict the risk of CKD progression in other races.

CKD is a progressive disease, associated with pathological accumulation of myofibroblasts that secrete ECM, leading to decline of renal function, and, ultimately, end stage renal failure. Clinically, there are no effective therapies to prevent or slow the progression of CKD. Therefore, it is imperative to discover therapeutic targets. Here, we showed that excess production of LIF by activated renal interstitial fibroblast is a robust feature of CKD, and inhibition of LIF signaling was effective in reducing TIF. LIF utilizes a receptor complex that consists of the LIFR and gp130 which is also used by CNTF, OSM, CT1 and CLCF1. Moreover, LIFR is broadly expressed in a number of different organs.[26] In addition, LIF is not expressed at detectable amounts in healthy adult tissues. Therefore, we assume that LIF is a more specific therapeutic target than LIFR. LIF knockout mice have a rather restricted set of development defects including loss of female fertility, endocrine system abnormalities and defects in some neurons and glial populations, and do not suffer from infections, cardiovascular disease, or cancer.[11,26,89,90] On the other hand, LIF is overexpressed and exerts an oncogenic function in many types of solid tumors.[91–94] Therefore, targeting LIF is not expected to be associated with serious side effects. It has been reported that a humanized anti-LIF antibody (MSC-1) was tested in a phase I clinical trial and was found to be safe and tolerated at doses from 75 to 1500 mg in patients with advanced solid tumors (ClinicalTrials.gov, NCT03490669). The most common treatment-related adverse events are fatigue and nausea.[95] It is possible that MSC-1 is a therapeutic candidate for CKD patients. Besides, a couple of small molecules targeting LIF/LIFR axis including EC330, EC357, EC363 have been developed (US patent 10,053,485). It is necessary to examine their therapeutic effect on TIF.[96]

Collectively, we propose that LIF is a critical molecule in driving TIF and a potential therapeutic target of CKD. In the current study, we proved that anti-LIF antibody is effective in attenuating TIF.

Contributors

J. Nie and F.F. Hou designed the study. S.H. Xu and J. Nie wrote the manuscript. S.H. Xu, Q. Z. Chen and Y. Chen performed in vitro experiments and data analysis. S.H. Xu, Q. Z. Chen and Y. Chen performed animal experiments and data analysis. J. Nie, F.F. Hou, X.B. Yang and X. Xu were involved in designing and developing the human kidney disease cohort. Z.L. Liu, X.T. Yao, L. L. Xie and S.H. Xu analyzed the clinical data. J.W. Tian measured uLIF of CKD patients. M.M. Zhou processed kidney samples and conducted histological analysis. Z.L. Liu and A. Xiao analyzed the published RNA-seq data. F.X. Zhu and F.F. Hou edited the manuscript. Z. Hu and M.M. Zhou provided reagents and technique support. All authors read, verified the underlying data and approved the final version of the manuscript. J. Nie and F.F. Hou were responsible for the decision to submit the manuscript.

Data sharing statement

Published RNA-seq and MS data of mice in the paper are from GEO under accession nos. GSE98622, GSE118339 and GSE126182. The data of UUO snRNA-seq (10X) are from GEO under accession nos. GSE119531 and UUO PDGFRβ^{+} scRNA-seq (SmartSeq2) are from https://zenodo.org/record/4059315 (https://doi.org/10.5281/zenodo.4059315). Published RNA-seq data of human are from Nephroseq (https://www.nephroseq.org). RNA-seq data of primary tubular epithelial cell are deposited in the National Genomics Data Center (NGDC), Genome Sequence Archive (GSA) database (https://bigd.big.ac.cn/gsa/) under accession number of CRA007647. RNA-seq data of patients in CKD are deposited in NGDC under accession number of HRA002764.

The data for this study are available by contacting the corresponding author upon reasonable request.

Declaration of interests

All the authors declared no conflict of interest.

Acknowledgments

This work was supported by grants from National Key R&D program of China (2020YFC2005000), Nature and Science Foundation of China (81730019, 81521003, 82090020), Nature and Science Foundation of Guangdong province (2019B1515120075) and Outstanding Scholar Program of Guangzhou Regenerative Medicine and Health Guangdong

at day 14 after UUO (f) and at day 12 after UIRI (g). (h) H-score of F4/80 and CD206 staining at day 7, 14 after UUO and day 12 after UIRI. $^{\#}P < 0.05$, $^{*}P < 0.01$ versus UUO7d-Lenti-GFP-NC, UUO14d-IgG and UIRI-12d-IgG, respectively (n = 6). (i) Schematic presentation the role of LIF in macrophages and in the crosstalk between renal fibroblasts and renal tubular epithelial cells and the mechanism to pro-fibrotic response during renal fibrosis. Data were expressed as means ± SD. Student's t-test was used for determining the *P* values while comparing between each pair of groups, respectively. $^{\#}P < 0.05$, $^{*}P < 0.01$.

Laboratory (2018GZR110102004) to Dr. Jing Nie, grant from the Nature and Science Foundation of China (82170700) to Dr. Fengxin Zhu, grant from the Nature and Science Foundation of China (82100784) to Dr. Liling Xie, grant from the National Natural Science Foundation of China (81970666) to Dr. Xiaobing Yang; grants from the National Natural Science Foundation of China (Key Program) (82030022) and Guangzhou Regenerative Medicine and Health-Guangdong Laboratory Research Grant (2018GZR0201003) to Dr. Fanfan Hou. We thank Professor Youhua liu for providing NRK49F cells.

Appendix A. Supplementary data

Supplementary data related to this article can be found at https://doi.org/10.1016/j.ebiom.2022.104312.

References

1 Chen TK, Knicely DH, Grams ME. Chronic kidney disease diagnosis and management: a review. *JAMA*. 2019;322(13):1294–1304. https://doi.org/10.1001/jama.2019.14745.
2 Kakitapalli Y, Ampolu J, Madasu SD, Sai KM. Detailed review of chronic kidney disease. *Kidney Dis (Basel)*. 2020;6(2):85–91. https://doi.org/10.1159/000504622.
3 Liu Y. Cellular and molecular mechanisms of renal fibrosis. *Nat Rev Nephrol*. 2011;7(12):684–696. https://doi.org/10.1038/nrneph.2011.149.
4 Djudjaj S, Boor P. Cellular and molecular mechanisms of kidney fibrosis. *Mol Aspects Med*. 2019;65:16–36. https://doi.org/10.1016/j.mam.2018.06.002.
5 Lebleu VS, Taduri G, O'Connell J, et al. Origin and function of myofibroblasts in kidney fibrosis. *Nat Med*. 2013;19(8):1047–1053. https://doi.org/10.1038/nm.3218.
6 Zhou Y, Xiong M, Niu J, et al. Secreted fibroblast-derived mir-34a induces tubular cell apoptosis in fibrotic kidney. *J Cell Sci*. 2014;127(Pt 20):4494–4506. https://doi.org/10.1242/jcs.155523.
7 O'Connor JW, Gomez EW. Biomechanics of tgfβ-induced epithelial-mesenchymal transition: implications for fibrosis and cancer. *Clin Transl Med*. 2014;3:23. https://doi.org/10.1186/2001-1326-3-23.
8 Lin L, Shi C, Sun Z, Le NT, Abe JI, Hu K. The ser/thr kinase p90rsk promotes kidney fibrosis by modulating fibroblast-epithelial crosstalk. *J Biol Chem*. 2019;294(25):9901–9910. https://doi.org/10.1074/jbc.RA119.007904.
9 Tan RJ, Zhou D, Liu Y. Signaling crosstalk between tubular epithelial cells and interstitial fibroblasts after kidney injury. *Kidney Dis (Basel)*. 2016;2(3):136–144. https://doi.org/10.1159/000446336.
10 Rudman-Melnick V, Adam M, Potter A, et al. Single-cell profiling of aki in a murine model reveals novel transcriptional signatures, profibrotic phenotype, and epithelial-to-stromal crosstalk. *J Am Soc Nephrol*. 2020;31(12):2793–2814. https://doi.org/10.1681/ASN.2020010052.
11 Rose-John S. Interleukin-6 family cytokines. *Cold Spring Harb Perspect Biol*. 2018;10(2). https://doi.org/10.1101/cshperspect.a028415.
12 West NR. Coordination of immune-stroma crosstalk by il-6 family cytokines. *Front Immunol*. 2019;10:1093. https://doi.org/10.3389/fimmu.2019.01093.
13 Kang S, Tanaka T, Narazaki M, Kishimoto T. Targeting interleukin-6 signaling in clinic. *Immunity*. 2019;50(4):1007–1023. https://doi.org/10.1016/j.immuni.2019.03.026.
14 Deisseroth A, Ko CW, Nie L, et al. FDA approval: siltuximab for the treatment of patients with multicentric castleman disease. *Clin Cancer Res*. 2015;21(5):950–954. https://doi.org/10.1158/1078-0432.CCR-14-1678.
15 Dai J, Lin D, Zhang J, et al. Chronic alcohol ingestion induces osteoclastogenesis and bone loss through il-6 in mice. *J Clin Invest*. 2000;106(7):887–895. https://doi.org/10.1172/JCI10483.
16 Naugler WE, Karin M. The wolf in sheep's clothing: the role of interleukin-6 in immunity, inflammation and cancer. *Trends Mol Med*. 2008;14(3):109–119. https://doi.org/10.1016/j.molmed.2007.12.007.
17 Fonseca JE, Santos MJ, Canhão H, Choy E. Interleukin-6 as a key player in systemic inflammation and joint destruction. *Autoimmun Rev*. 2009;8(7):538–542. https://doi.org/10.1016/j.autrev.2009.01.012.
18 Ataie-Kachoie P, Pourgholami MH, Morris DL. Inhibition of the il-6 signaling pathway: a strategy to combat chronic inflammatory diseases and cancer. *Cytokine Growth Factor Rev*. 2013;24(2):163–173. https://doi.org/10.1016/j.cytogfr.2012.09.001.
19 Yang J, Chen J, Yan J, et al. Effect of interleukin 6 deficiency on renal interstitial fibrosis. *PLoS One*. 2012;7(12):e52415. https://doi.org/10.1371/journal.pone.0052415.
20 Chen W, Yuan H, Cao W, et al. Blocking interleukin-6 trans-signaling protects against renal fibrosis by suppressing stat3 activation. *Theranostics*. 2019;9(14):3980–3991. https://doi.org/10.7150/thno.32352.
21 Schafer S, Viswanathan S, Widjaja AA, et al. Il-11 is a crucial determinant of cardiovascular fibrosis. *Nature*. 2017;552(7683):110–115. https://doi.org/10.1038/nature24676.
22 Ng B, Dong J, D'Agostino G, et al. Interleukin-11 is a therapeutic target in idiopathic pulmonary fibrosis. *Sci Transl Med*. 2019;11(511). https://doi.org/10.1126/scitranslmed.aaw1237.
23 Morita Y, Masters EA, Schwarz EM, Muthukrishnan G. Interleukin-27 and its diverse effects on bacterial infections. *Front Immunol*. 2021;12:678515. https://doi.org/10.3389/fimmu.2021.678515.
24 Aparicio-Siegmund S, Garbers C. The biology of interleukin-27 reveals unique pro- and anti-inflammatory functions in immunity. *Cytokine Growth Factor Rev*. 2015;26(5):579–586. https://doi.org/10.1016/j.cytogfr.2015.07.008.
25 Coppock GM, Aronson LR, Park J, et al. Loss of il-27rα results in enhanced tubulointerstitial fibrosis associated with elevated th17 responses. *J Immunol*. 2020;205(2):377–386. https://doi.org/10.4049/jimmunol.1901463.
26 Nicola NA, Babon JJ. Leukemia inhibitory factor (lif). *Cytokine Growth Factor Rev*. 2015;26(5):533–544. https://doi.org/10.1016/j.cytogfr.2015.07.001.
27 Magno AL, Herat LY, Carnagarin R, Schlaich MP, Matthews VB. Current knowledge of il-6 cytokine family members in acute and chronic kidney disease. *Biomedicines*. 2019;7(1):19. https://doi.org/10.3390/biomedicines7010019.
28 Dai Y, Zhang W, Wen J, Zhang Y, Kellems RE, Xia Y. A2b adenosine receptor-mediated induction of il-6 promotes ckd. *J Am Soc Nephrol*. 2011;22(5):890–901. https://doi.org/10.1681/ASN.2010080890.
29 Nightingale J, Patel S, Suzuki N, et al. Oncostatin m, a cytokine released by activated mononuclear cells, induces epithelial cell-myofibroblast transdifferentiation via jak/stat pathway activation. *J Am Soc Nephrol*. 2004;15(1):21–32. https://doi.org/10.1097/01.asn.0000102479.92582.43.
30 Savin VJ, Sharma M, Zhou J, et al. Renal and hematological effects of clcf-1, a b-cell-stimulating cytokine of the il-6 family. *J Immunol Res*. 2015;2015:714964. https://doi.org/10.1155/2015/714964.
31 Liu J, Kumar S, Dolzhenko E, et al. Molecular characterization of the transition from acute to chronic kidney injury following ischemia/reperfusion. *JCI Insight*. 2017;2(18):e94716. https://doi.org/10.1172/jci.insight.94716.
32 Pavkovic M, Pantano L, Gerlach CV, et al. Multi omics analysis of fibrotic kidneys in two mouse models. *Sci Data*. 2019;6(1):92. https://doi.org/10.1038/s41597-019-0095-5.
33 Bolger AM, Lohse M, Usadel B. Trimmomatic: a flexible trimmer for illumina sequence data. *Bioinformatics*. 2014;30(15):2114–2120. https://doi.org/10.1093/bioinformatics/btu170.
34 Chen S, Zhou Y, Chen Y, Gu J. Fastp: an ultra-fast all-in-one fastq preprocessor. *Bioinformatics*. 2018;34(17):i884–i890. https://doi.org/10.1093/bioinformatics/bty560.
35 Liao Y, Smyth GK, Shi W. Featurecounts: an efficient general-purpose program for assigning sequence reads to genomic features. *Bioinformatics*. 2014;30(7):923–930. https://doi.org/10.1093/bioinformatics/btt656.
36 Ritchie ME, Phipson B, Wu D, et al. Limma powers differential expression analyses for rna-sequencing and microarray studies. *Nucleic Acids Res*. 2015;43(7):e47. https://doi.org/10.1093/nar/gkv007.
37 Subramanian A, Tamayo P, Mootha VK, et al. Gene set enrichment analysis: a knowledge-based approach for interpreting genome-wide expression profiles. *Proc Natl Acad Sci U S A*. 2005;102(43):15545–15550. https://doi.org/10.1073/pnas.0506580102.
38 Hänzelmann S, Castelo R, Guinney J. Gsva: gene set variation analysis for microarray and rna-seq data. *BMC Bioinformatics*. 2013;14:7. https://doi.org/10.1186/1471-2105-14-7.
39 Wu H, Kirita Y, Donnelly EL, Humphreys BD. Advantages of single-nucleus over single-cell rna sequencing of adult kidney: rare cell types and novel cell states revealed in fibrosis. *J Am Soc Nephrol*. 2019;30(1):23–32. https://doi.org/10.1681/ASN.2018090912.
40 Kuppe C, Ibrahim MM, Kranz J, et al. Decoding myofibroblast origins in human kidney fibrosis. *Nature*. 2021;589(7841):281–286. https://doi.org/10.1038/s41586-020-2941-1.

41 Satija R, Farrell JA, Gennert D, Schier AF, Regev A. Spatial reconstruction of single-cell gene expression data. *Nat Biotechnol*. 2015;33(5):495–502. https://doi.org/10.1038/nbt.3192.

42 Stuart T, Butler A, Hoffman P, et al. Comprehensive integration of single-cell data. *Cell*. 2019;177(7):1888–1902.e21. https://doi.org/10.1016/j.cell.2019.05.031.

43 Chang X, Zhen X, Liu J, et al. The antihelmenthic phosphate niclosamide impedes renal fibrosis by inhibiting homeodomain-interacting protein kinase 2 expression. *Kidney Int*. 2017;92(3):612–624. https://doi.org/10.1016/j.kint.2017.01.018.

44 Li S, Qiu B, Lu H, et al. Hyperhomocysteinemia accelerates acute kidney injury to chronic kidney disease progression by down-regulating heme oxygenase-1 expression. *Antioxid Redox Signal*. 2019;30(13):1635–1650. https://doi.org/10.1089/ars.2017.7397.

45 Zhou D, Li Y, Zhou L, et al. Sonic hedgehog is a novel tubule-derived growth factor for interstitial fibroblasts after kidney injury. *J Am Soc Nephrol*. 2014;25(10):2187–2200. https://doi.org/10.1681/ASN.2013080893.

46 Hu K, Lin L, Tan X, et al. Tpa protects renal interstitial fibroblasts and myofibroblasts from apoptosis. *J Am Soc Nephrol*. 2008;19(3):503–514. https://doi.org/10.1681/ASN.2007030300.

47 Wu W, Liu C, Farrar CA, et al. Collectin-11 promotes the development of renal tubulointerstitial fibrosis. *J Am Soc Nephrol*. 2018;29(1):168–181. https://doi.org/10.1681/ASN.2017050544.

48 Chiba T, Peasley KD, Cargill KR, et al. Sirtuin 5 regulates proximal tubule fatty acid oxidation to protect against aki. *J Am Soc Nephrol*. 2019;30(12):2384–2398. https://doi.org/10.1681/ASN.2019020163.

49 Maimon A, Levi-Yahid V, Ben-Meir K, et al. Myeloid cell-derived pros1 inhibits tumor metastasis by regulating inflammatory and immune responses via il-10. *J Clin Invest*. 2021;131(10):e126089. https://doi.org/10.1172/JCI126089.

50 Taupin JL, Morel D, Moreau JF, Gualde N, Potaux L, Bezian JH. Hilda/lif urinary excretion during acute kidney rejection. *Transplantation*. 1992;53(3):655–658. https://doi.org/10.1097/00007890-199203000-00031.

51 Ding H, Zhou D, Hao S, et al. Sonic hedgehog signaling mediates epithelial-mesenchymal communication and promotes renal fibrosis. *J Am Soc Nephrol*. 2012;23(5):801–813. https://doi.org/10.1681/ASN.2011060614.

52 Sakakini N, Turchi L, Bergon A, et al. A positive feed-forward loop associating egr1 and pdgfa promotes proliferation and self-renewal in glioblastoma stem cells. *J Biol Chem*. 2016;291(20):10684–10699. https://doi.org/10.1074/jbc.M116.720698.

53 Marquardt RM, Kim TH, Yoo JY, et al. Endometrial epithelial arid1a is critical for uterine gland function in early pregnancy establishment. *FASEB J*. 2021;35(2):e21209. https://doi.org/10.1096/fj.202002178R.

54 Laszlo GS, Nathanson NM. Src family kinase-independent signal transduction and gene induction by leukemia inhibitory factor. *J Biol Chem*. 2003;278(30):27750–27757. https://doi.org/10.1074/jbc.M303670200.

55 Liang XH, Deng WB, Li M, et al. Egr1 protein acts downstream of estrogen-leukemia inhibitory factor (lif)-stat3 pathway and plays a role during implantation through targeting wnt4. *J Biol Chem*. 2014;289(34):23534–23545. https://doi.org/10.1074/jbc.M114.588897.

56 Yadav S, Pant D, Samaiya A, Kalra N, Gupta S, Shukla S. Erk1/2-egr1-srsf10 axis mediated alternative splicing plays a critical role in head and neck cancer. *Front Cell Dev Biol*. 2021;9:713661. https://doi.org/10.3389/fcell.2021.713661.

57 Hwang DB, Kim SY, Won DH, et al. Egr1 gene expression as a potential biomarker for in vitro prediction of ocular toxicity. *Pharmaceutics*. 2021;13(10):1584. https://doi.org/10.3390/pharmaceutics13101584.

58 Rouillard AD, Gundersen GW, Fernandez NF, et al. The harmonizome: a collection of processed datasets gathered to serve and mine knowledge about genes and proteins. *Database (Oxford)*. 2016;2016:baw100. https://doi.org/10.1093/database/baw100.

59 Böing I, Stross C, Radtke S, Lippok BE, Heinrich PC, Hermanns HM. Oncostatin m-induced activation of stress-activated map kinases depends on tyrosine 861 in the osm receptor and requires jak1 but not src kinases. *Cell Signal*. 2006;18(1):50–61. https://doi.org/10.1016/j.cellsig.2005.03.015.

60 Liu J, Shoyab M, Grove RI. Induction of egr-1 by oncostatin m precedes up-regulation of lowdensity lipoprotein receptors in hepg2 cells. *Cell Growth Differ*. 1993;4(7):611–616.

61 Elbjeirami WM, Truong LD, Tawil A, et al. Early differential expression of oncostatin m in obstructive nephropathy. *J Interferon Cytokine Res*. 2010;30(7):513–523. https://doi.org/10.1089/jir.2009.0105.

62 Tang PM, Nikolic-Paterson DJ, Lan HY. Macrophages: versatile players in renal inflammation and fibrosis. *Nat Rev Nephrol*. 2019;15(3):144–158. https://doi.org/10.1038/s41581-019-0110-2.

63 Eiken HG, øie E, Damås JK, et al. Myocardial gene expression of leukaemia inhibitory factor, interleukin-6 and glycoprotein 130 in end-stage human heart failure. *Eur J Clin Invest*. 2001;31(5):389–397. https://doi.org/10.1046/j.1365-2362.2001.00795.x.

64 Kodama H, Fukuda K, Pan J, et al. Leukemia inhibitory factor, a potent cardiac hypertrophic cytokine, activates the jak/stat pathway in rat cardiomyocytes. *Circ Res*. 1997;81(5):656–663. https://doi.org/10.1161/01.res.81.5.656.

65 Kanazawa H, Ieda M, Kimura K, et al. Heart failure causes cholinergic transdifferentiation of cardiac sympathetic nerves via gp130-signaling cytokines in rodents. *J Clin Invest*. 2010;120(2):408–421. https://doi.org/10.1172/JCI39778.

66 Wu D, Guo J, Qi B, Xiao H. Tgf-β1 induced proliferation, migration, and ecm accumulation through the snhg11/mir-34b/lif pathway in human pancreatic stellate cells. *Endocr J*. 2021;68(11):1347–1357. https://doi.org/10.1507/endocrj.EJ21-0176.

67 Bamber BA, Masters BA, Hoyle GW, Brinster RL, Palmiter RD. Leukemia inhibitory factor induces neurotransmitter switching in transgenic mice. *Proc Natl Acad Sci U S A*. 1994;91(17):7839–7843. https://doi.org/10.1073/pnas.91.17.7839.

68 Matsumoto K, Xavier S, Chen J, et al. Instructive role of the microenvironment in preventing renal fibrosis. *Stem Cells Transl Med*. 2017;6(3):992–1005. https://doi.org/10.5966/sctm.2016-0095.

69 Yoshino J, Monkawa T, Tsuji M, Hayashi M, Saruta T. Leukemia inhibitory factor is involved in tubular regeneration after experimental acute renal failure. *J Am Soc Nephrol*. 2003;14(12):3090–3101. https://doi.org/10.1097/01.asn.0000101180.96787.02.

70 Knight MN, Hankenson KD. R-spondins: novel matricellular regulators of the skeleton. *Matrix Biol*. 2014;37:157–161. https://doi.org/10.1016/j.matbio.2014.06.003.

71 He L, Wei Q, Liu J, et al. Aki on ckd: heightened injury, suppressed repair, and the underlying mechanisms. *Kidney Int*. 2017;92(5):1071–1083. https://doi.org/10.1016/j.kint.2017.06.030.

72 Xiao L, Zhou D, Tan RJ, et al. Sustained activation of wnt/β-catenin signaling drives aki to ckd progression. *J Am Soc Nephrol*. 2016;27(6):1727–1740. https://doi.org/10.1681/ASN.2015040449.

73 Yu Y, Wang Y, Niu Y, Fu L, Chin YE, Yu C. Leukemia inhibitory factor attenuates renal fibrosis through stat3-mir-29c. *Am J Physiol Renal Physiol*. 2015;309(7):F595–F603. https://doi.org/10.1152/ajprenal.00634.2014.

74 Yang B, Janardhanan R, Vohra P, et al. Adventitial transduction of lentivirus-shrna-vegf-a in arteriovenous fistula reduces venous stenosis formation. *Kidney Int*. 2014;85(2):289–306. https://doi.org/10.1038/ki.2013.290.

75 Naito M, Shenoy A, Aoyama I, et al. High ambient glucose augments angiotensin ii-induced proinflammatory gene mrna expression in human mesangial cells: effects of valsartan and simvastatin. *Am J Nephrol*. 2009;30(2):99–111. https://doi.org/10.1159/000203619.

76 Wang X, Shaw S, Amiri F, Eaton DC, Marrero MB. Inhibition of the jak/stat signaling pathway prevents the high glucose-induced increase in tgf-beta and fibronectin synthesis in mesangial cells. *Diabetes*. 2002;51(12):3505–3509. https://doi.org/10.2337/diabetes.51.12.3505.

77 Hartner A, Goppelt-Struebe M, Hocke GM, Sterzel RB. Differential regulation of chemokines by leukemia inhibitory factor, interleukin-6 and oncostatin m. *Kidney Int*. 1997;51(6):1754–1760. https://doi.org/10.1038/ki.1997.241.

78 Shen MM, Skoda RC, Cardiff RD, Campos-Torres J, Leder P, Ornitz DM. Expression of lif in transgenic mice results in altered thymic epithelium and apparent interconversion of thymic and lymph node morphologies. *EMBO J*. 1994;13(6):1375–1385.

79 Friedrich B, Janessa A, Artunc F, et al. Doca and tgf-beta induce early growth response gene-1 (egr-1) expression. *Cell Physiol Biochem*. 2008;22(5–6):465–474. https://doi.org/10.1159/000185495.

80 Ohba M, Shibanuma M, Kuroki T, Nose K. Production of hydrogen peroxide by transforming growth factor-beta 1 and its involvement in induction of egr-1 in mouse osteoblastic cells. *J Cell Biol*. 1994;126(4):1079–1088. https://doi.org/10.1083/jcb.126.4.1079.

81 Shin SJ, Hang HT, Thang BQ, et al. Role of par1-egr1 in the initiation of thoracic aortic aneurysm in fbln4-deficient mice. *Arterioscler Thromb Vasc Biol*. 2020;40(8):1905–1917. https://doi.org/10.1161/ATVBAHA.120.314560.

82 Jung SN, Oh C, Chang JW, et al. Egr1/gadd45α activation by ros of non-thermal plasma mediates cell death in thyroid

carcinoma. *Cancers (Basel)*. 2021;13(2):351. https://doi.org/10.3390/cancers13020351.
83 Shi L, Kishore R, Mcmullen MR, Nagy LE. Lipopolysaccharide stimulation of erk1/2 increases tnf-alpha production via egr-1. *Am J Physiol Cell Physiol*. 2002;282(6):C1205–C1211. https://doi.org/10.1152/ajpcell.00511.2001.
84 Nguyen HN, Noss EH, Mizoguchi F, et al. Autocrine loop involving il-6 family member lif, lif receptor, and stat4 drives sustained fibroblast production of inflammatory mediators. *Immunity*. 2017;46(2):220–232. https://doi.org/10.1016/j.immuni.2017.01.004.
85 Kosfeld A, Brand F, Weiss AC, et al. Mutations in the leukemia inhibitory factor receptor (lifr) gene and lifr deficiency cause urinary tract malformations. *Hum Mol Genet*. 2017;26(9):1716–1731. https://doi.org/10.1093/hmg/ddx086.
86 Watanabe Y, Hashimoto S, Kakita A, et al. Neonatal impact of leukemia inhibitory factor on neurobehavioral development in rats. *Neurosci Res*. 2004;48(3):345–353. https://doi.org/10.1016/j.neures.2003.12.001.
87 Akita S, Malkin J, Melmed S. Disrupted murine leukemia inhibitory factor (lif) gene attenuates adrenocorticotropic hormone (acth) secretion. *Endocrinology*. 1996;137(7):3140–3143. https://doi.org/10.1210/endo.137.7.8770940.
88 Barasch J, Yang J, Ware CB, et al. Mesenchymal to epithelial conversion in rat metanephros is induced by lif. *Cell*. 1999;99(4):377–386. https://doi.org/10.1016/s0092-8674(00)81524-x.
89 Bugga L, Gadient RA, Kwan K, Stewart CL, Patterson PH. Analysis of neuronal and glial phenotypes in brains of mice deficient in leukemia inhibitory factor. *J Neurobiol*. 1998;36(4):509–524. https://doi.org/10.1002/(sici)1097-4695(19980915)36:4<509::aid-neu5>3.0.co;2-#.
90 Spangenburg EE, Booth FW. Leukemia inhibitory factor restores the hypertrophic response to increased loading in the lif(-/-) mouse. *Cytokine*. 2006;34(3–4):125–130. https://doi.org/10.1016/j.cyto.2006.05.001.
91 Shi Y, Gao W, Lytle NK, et al. Targeting lif-mediated paracrine interaction for pancreatic cancer therapy and monitoring. *Nature*. 2019;569(7754):131–135. https://doi.org/10.1038/s41586-019-1130-6.
92 Pascual-García M, Bonfill-Teixidor E, Planas-Rigol E, et al. Lif regulates cxcl9 in tumor-associated macrophages and prevents cd8(+) t cell tumor-infiltration impairing anti-pd1 therapy. *Nat Commun*. 2019;10(1):2416. https://doi.org/10.1038/s41467-019-10369-9.
93 Li X, Yang Q, Yu H, et al. Lif promotes tumorigenesis and metastasis of breast cancer through the akt-mtor pathway. *Oncotarget*. 2014;5(3):788–801. https://doi.org/10.18632/oncotarget.1772.
94 Albrengues J, Bourget I, Pons C, et al. Lif mediates proinvasive activation of stromal fibroblasts in cancer. *Cell Rep*. 2014;7(5):1664–1678. https://doi.org/10.1016/j.celrep.2014.04.036.
95 Borazanci E, Schram AM, Garralda E, et al. Phase i, first-in-human study of msc-1 (azd0171), a humanized anti-leukemia inhibitory factor monoclonal antibody, for advanced solid tumors. *ESMO Open*. 2022;7(4):100530. https://doi.org/10.1016/j.esmoop.2022.100530.
96 Viswanadhapalli S, Dileep KV, Zhang K, Nair HB, Vadlamudi RK. Targeting lif/lifr signaling in cancer. *Genes Dis*. 2022;9(4):973–980. https://doi.org/10.1016/j.gendis.2021.04.003.